UCRL-1447

UNCLASSIFIED

UNIVERSITY OF CALIFORNIA — BERKELEY

TWO-WEEK LOAN COPY

This is a Library Circulating Copy which may be borrowed for two weeks. For a personal retention copy, call Tech. Info. Division, Ext. 5545

RADIATION LABORATORY

DISCLAIMER

This document was prepared as an account of work sponsored by the United States Government. While this document is believed to contain correct information, neither the United States Government nor any agency thereof, nor the Regents of the University of California, nor any of their employees, makes any warranty, express or implied, or assumes any legal responsibility for the accuracy, completeness, or usefulness of any information, apparatus, product, or process disclosed, or represents that its use would not infringe privately owned rights. Reference herein to any specific commercial product, process, or service by its trade name, trademark, manufacturer, or otherwise, does not necessarily constitute or imply its endorsement, recommendation, or favoring by the United States Government or any agency thereof, or the Regents of the University of California. The views and opinions of authors expressed herein do not necessarily state or reflect those of the United States Government or any agency thereof or the Regents of the University of California.

UCRL-1447
Unclassified-Physics

UNIVERSITY OF CALIFORNIA

Radiation Laboratory

Contract No. W-7405-eng-48

THE DIFFERENTIAL CROSS SECTION FOR THE SCATTERING OF 9.5 MEV PROTONS FROM HELIUM

Thomas Milton Putnam, Jr.
(Thesis)

August 22, 1951

Berkeley, California

TABLE OF CONTENTS

CHAPTER		PAGE
I	INTRODUCTION	1
II	ASSOCIATED THEORY	4
III	APPARATUS	15
IV	NUCLEAR EMULSION TECHNIQUE	26
V	EXPERIMENTAL PROCEDURE	47
VI	BEAM POSITION AND ENERGY	69
VII	EXPERIMENTAL RESULTS	72

APPENDICES

I	DERIVATION OF THE CRITCHFIELD FORMULA	83
II	COLLISION MECHANICS FOR NUCLEAR SCATTERING	90
III	EXPERIMENTAL DATA	96
IV	COULOMB SCATTERING	98

ACKNOWLEDGMENTS 102

BIBLIOGRAPHY 103

PHOTOGRAPHS AND DRAWINGS

FIGURE		PAGE
1	Slit System Geometry - Schematic	7
2	Cyclotron and Camera - Schematic	16
3	Cyclotron, Snout, and Camera Arrangement - Photograph	19
4	Multi-Plate Camera - Schematic	21
5	Camera Pump and Gas Handling System - Schematic	25
6	Microscope Laboratory Arrangement - Photograph	31
7	Microscope Super-Stage - Drawing	33
8	Microscope Super-Stage - Observers View - Photograph	35
9	Microscope Super-Stage - Light Source Side - Photograph	37
10	Track Density Distribution 20°	39
11	Track Density Distribution 150°	40
12	Track Range Distribution 20°	42
13	Track Range Distribution 150°	43
14	Multiplate Camera - S. Side - Photograph	50
15	Multiplate Camera and Plates - Photograph	53
16	Multiplate Camera and Plates - Photograph	55
17	Multiplate Camera Assembly - Photograph	59
18	Multiplate Camera - Photograph	61
19	Current Integration Circuit - Schematic	65
20	Current Integration Equipment - Photograph	67
21	Differential Cross Section Curve	75
22	Comparison of Differential Cross Sections at Various Energies	78
23	Slit Geometry and the Similar Triangles Formed	84

CHAPTER I

INTRODUCTION

The scattering of protons from helium nuclei has several aspects which are of fundamental interest in nuclear physics. First of all, there is the possible information which the angular distribution of the scattered products can give to aid in forming a theory of nuclear forces. The scattering of protons from light nuclei has yielded much of the information on which the present theories of nuclear forces are based. At present, however, the theoretical interpretation of the scattering of protons from helium is limited to the treatment by phase shift analysis. The phase shift analysis of the proton-helium scattering at lower energies [1] (up to 3.6-Mev) indicates that S and P wave scattering is present but there is no evidence of anomalous phase shifts of higher angular momenta. The P wave phase shifts are apparently double valued but it is not possible with the data available at present to determine whether the doublet (in Li^5) is normal or inverted. The data at higher energies may help to clarify this situation.

The second point of interest is in the search for excited states of the ~~compound~~ nucleus ~~Li^5~~ He^4. The reaction involved here is:

$$He^4 + H^1 \longrightarrow Li^{5*} \longrightarrow He^4_s + H^1_s$$

If one considers this reaction together with that of the elastic scattering, which may be written $He^4 + H^1 \longrightarrow He_s^4 + H_s^1$ then two or more ranges of protons should be observed at any particular scattering angle, within certain energy limits. Thus, the existence of two groups of protons would give some information on an excited state in ~~Li^5~~ He^4. As will be mentioned later, no such effect was observed. However, it is possible

---

[1] C. L. Critchfield and D. C. Dodder, Phys. Rev. 76, 602 (1949).

that the incident proton energy is too high for the state to be observed.

In previous investigations[2,3], emphasis has been placed on establishing the existence of resonance scattering due to an excited state of the compound nucleus. A broad resonance in the backward scattering was observed in the neighborhood of 2-Mev incident proton energy. Earlier work in the field was limited by the maximum available proton energy. Heydenburg and Roberts[4] used protons up to 1-Mev in energy while in the earlier experiments on the scattering of alpha-particles by hydrogen[5,6], the maximum available alpha-particle energy was 8.5-Mev. This corresponds to a maximum indicent proton energy of 2.1-Mev. Thus, in this work the available energy was too low to ovserve the resonance effect.

In the present work the scattering measurements were limited to one incident energy, that of 9.5-Mev. However, the existence of inelastic scattering could be established as mentioned above since nuclear research emulsions were used for the detection of the scattered particles. Since the emulsion is continuously sensitive to all ranges of particles, a permanent record is provided of all the scattered products that appeared under the conditions of a particular run. Thus, if there are two ranges of protons present in reasonable numbers, these would be detected. With this data, the energy range investigated for the scattering of protons by helium

---

2 N. P. Heyenburg and N. F. Ramsey, Phys. Rev. 60, 42 (1941).

3 G. Freier, E. Lampi, W. Sleator and J. H. Williams, Phys. Rev. 75, 1345 (1949).

4 N. P. Heydenburg and R. B. Roberts, Phys. Rev. 56, 1092 (1939).

5 J. Chadwick and E. S. Bieler, Phil. Mag. 92, 923 (1921).

6 C. B. O. Mohr and G. E. Pringle, Proc. Roy. Soc. 160, 190 (1937).

nuclei has been extended from 3.5-Mev to 9.5-Mev. The angular range covered has also been extended to 172.5 degrees in the laboratory coordinates. Also, sufficient points have been measured to rule out the existence of any fine structure in the angular distribution curve.

The general nature of the present experiment was the scattering of 9.5-Mev protons from a "thin" helium gas target and the measurement of the angular distribution of the scattered products by means of nuclear emulsions. The 20-Mev molecular hydrogen beam from the 60" cyclotron in Crocker Laboratory was used as the source of the protons. The scattering chamber and associated equipment, which was developed at the Los Alamos Scientific Laboratories [7], was used in the present work with the kind permission and assistance of Dr. Louis Rosen.

---

[7] J. C. Allred, L. Rosen, F. K. Tallmadge, and J. H. Williams, Rev. Sci. Inst. 22, 191 (1951).

CHAPTER II

ASSOCIATED THEORY

1. The Cross Section Formula.

As already discussed, the experiment to be described involves the measurement of an angular distribution of particles scattered from nuclei in a region in the center of a scattering chamber. Distributions of this type are usually expressed in terms of the differential cross section per unit solid angle. This quantity may be considered to represent the effective geometrical cross section of a target (helium) nucleus to the incident beam of particles (protons) for the occurrence of the scattering process.

Let us consider first the basic concept of the cross section for the scattering process. The totoal number of scattered particles (Y) from a given process will be proportional to the number of incident particles in the beam per unit area (N) and the number of scattering centers (n_t). Thus, $y \propto Nn_t$. The constant of proportionality is known as the cross section for the process. Thus,

$$Y = \sigma N n_t ,$$

where σ is the total cross section. It also may be considered as the probability for the process to occur.

Another way to develop the concept of cross section is to consider a flux of N' particles/cm^3 moving with velocity v cm/sec. Then consider this incident on a foil containing n particles per cm^2. The rate for the process (i.e., the number of scattering events per second in this case) will be given by

$$R = \sigma n N' v ,$$

where σ again represents the total cross section for the process. If the total number of events is to be determined, we essentially multiply by the time of observation and obtain the same relation as above. Thus, to determine the total cross section for the process, one must determine the total number (flux) of particles incident on the target nuclei, the total number of scattering centers (target nuclei) per unit area and the total number of scattered particles produced.

In the measurements involved in this experiment, as a matter of experimental convenience, the process was observed at different angles to the beam and the angular distribution about the scattering center was determined in a plane which contains the beam. Essentially, in the measurement of total cross section discussed above, all particles at all angles have to be detected. In the measurement of an angular distribution, one observes the number of scattered particles which, in leaving the scattering volume, pass through the solid angle subtended by the detector at a given angle Θ. Thus, one measures the yield over a small element of the solid angle around the scattering center. The expression for this element of the total yield may be written

$$dy = nN \frac{d\sigma(\Theta)}{d\omega} d\omega ,$$

where $\frac{d\sigma(\Theta)}{d\omega}$ is the differential cross section per unit solid angle (steradian) and $d\omega$ is the element of solid angle. Thus, the element of yield which passes through the solid angle $d\omega$ subtended by the detector will give the differential cross section for the process involved.

In the above relation n is the number of target nuclei per cm^2.

To transform this to the case at hand, that of scattering from a volume of gas, the target foil may be considered as a cylinder along the axis of the beam of length λ and of radius small compared to the distance to the detector. Then we may write

$$dy = n_o \lambda N \frac{d\sigma(\theta)}{d\omega} d\omega .$$

Here n_o is the number of gas nuclei per unit volume and N is the total number of particles passing through the scattering volume. This assumes essentially a line source of scattering centers. Since the radius of the incident beam is approximately 3/32 inches and the distance to the detector is approximately eight inches, this would appear to be a valid approximation. It can be shown analytically[8] that the difference between the average solid angle subtended by the detector from the extreme edges of the beam and that subtended from the axis is completely negligible.

Let us consider now the geometry of the collimation system used in the experiment. Fig. 1 shows the essential details of this geometry. It can be seen from the figure that different elements of the scattering "volume" will have a different effectiveness in producing "counts" at the detector and that this effectiveness will vary with the angle of scattering. In order to determine this, consider an element dy of the scattering gas which is a distance y from the center of the scattering "volume". Suppose that an event takes place in this element and a proton enters the emulsion in an element of the plate of length dx and width w, this point being a distance x from the

---

8 J. C. Allred, Los Alamos Laboratory Report, LA-981 (1950).

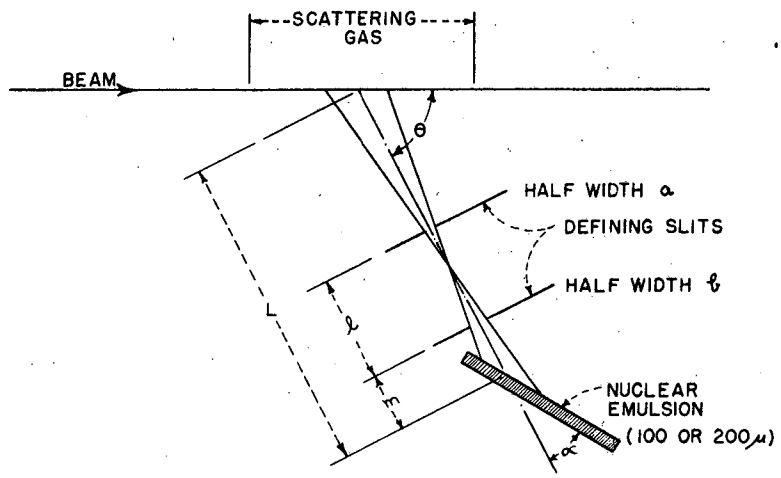

l = 2.875"
$a = b$ = 0.045"
α = 11° 46'

SLIT SYSTEM GEOMETRY

Figure 1

MU 2268

plate-slit axis. The number of scattering centers in the element dy along the axis of the beam is then $n_o dy$ particles per cm^2. Essentially dy is considered as the length which is effective in producing tracks at the point dx on the plate. Then the second differential element of yield may be written

$$d^2y = n_o N \frac{d\sigma(\theta)}{d\omega} dy d\omega .$$

If Y is the number of scattered particles detected on the plate, then

$$Y = n_o N \frac{d\sigma(\theta)}{d\omega} \iint dy d\omega .$$

If this number of particles are counted in a swath of width w and length dx along the plate, the element of area projected normal to the direction of the scattered particles is w dx sin ϕ , where ϕ is angle between the line between the elements dy and dx and the photographic plate. This represents an element of solid angle w dx sin ϕ/R^2 where R is the distance between dy and dx. Thus the yield is given by

$$Y = n_o N \frac{d\sigma(\theta)}{d\omega} \iint \frac{w \sin\phi}{R^2} dy dx.$$

To determine the cross section from the yield of tracks on the photographic plate detectors, the quantity

$$I = \iint \frac{w \sin\phi}{R^2} dy dx$$

must be evaluated.

The development of this quantity has been derived by Professor C. L. Critchfield of the University of Minnesota. The derivation is given in Appendix I. The result is:

$$Y = n_o N \frac{d\sigma(\theta)}{d\omega} \frac{4abw}{L\ell \sin\theta} \left\{ 1 - \frac{a^2 + b^2}{2\ell^2} - \frac{Pa^2 + Qb^2}{3\ell^2} \cot\alpha + \frac{Pa^2 + Qb^2}{3\ell^2} \right\} ,$$

where

$$P = \frac{m(\cot\alpha - \cot\theta)}{L} \; , \quad Q = \frac{(m + \ell)(\cot\alpha - \cot\theta)}{L} \; .$$

The geometrical quantities a, b, ℓ, m, L and α are shown in Fig. 1. Thus the determination of the differential cross section involves the measurement of the number of tracks per unit swath width, the total number of incident particles, and the number of target nuclei per cm^3 and the determination of a geometrical factor from the dimensions of the experimental equipment.

The geometrical correction factor (bracket term) to the cross section formula is very nearly unity. The maximum value, which occurs at approximately 90 degrees is less than 0.1 percent and, hence, can be neglected. The cross section formula may then be written:

$$\frac{d\,\sigma(\theta)}{d\omega} = \frac{Y}{W} \cdot \frac{\ell L \sin\theta}{n_o N a b} \; ,$$

where a and b now represent the full slit width, not the half width.

A rather simple qualitative derivation of the cross section formula may be obtained as follows[9]. Consider again the slits to be of width a and b (instead of 2a and 2b). To determine the effective number of scattering centers, project the first slit onto the beam axis. The length of the projection of this line is $a/\sin\theta$. Assume that on the average, particles that are scattered from nuclei along this line element, and that pass through the first slit, will pass through the

---

[9] J. C. Allred - Private communication.

second slit and be recorded on the plate. Thus, the effective number of scattering centers is $n_0 a/\sin\theta$. To determine the solid angle subtended by the detector at the scattering center, consider first the angle subtended by the second slit at the first. At each point of the first slit, the second slit will subtend approximately the same angle, i.e., b/ℓ. Since it has been assumed that particles coming from the line element and passing through the first slit will, on the average, pass through the second slit to be recorded by the detector, the angle subtended by the second slit at the first gives the horizontal component of the solid angle of the detector. The vertical component is the angle subtended by the swath on the detector of width w at the scattering center. This is w/L. Thus

$$d\omega = \frac{w}{L}\,\frac{b}{\ell}$$

and since

$$Y = n_0 N \lambda \frac{d\sigma(\theta)}{d\omega}\, d\omega ,$$

we have, substituting the expressions for λ and $d\omega$,

$$Y = \frac{n_0 N a b}{L \ell \sin\theta}\, w \frac{d\sigma(\theta)}{d\omega} ,$$

and

$$\frac{d\sigma(\theta)}{d\omega} = \frac{Y}{w} \cdot \frac{n_0 N a b}{\ell L \sin\theta} .$$

2. Mechanics of the Proton-Helium Collision.

In order that the proper interpretation of the data obtained from the nuclear plate detectors may be made, the fundamental aspects of the scattering of protons from helium nuclei are needed. The general mechanics for nuclear collisions in the non-relativistic range are derived in Appendix II with the particular relations for the proton helium case. The fundamental relations developed there and their interpretation will be given here.

In this experiment the primary purpose as discussed in Chapter I was the measurement of the angular distribution for the elastic scattering of protons. In addition the data was obtained in such a form that the effects of an excited state of the Li^5 nucleus could be observed. Since there was no indication in the data of inelastic collisions, these will not be discussed. For the elastic collision of high energy protons with the helium gas, because of the energy (or velocity) of the incident particles (protons), the target nuclei (helium) can be assumed at rest in the laboratory coordinate system. This is the system, at rest with respect to the observer, in which the experiment was performed. The angles of stattering are the angles defined by the camera slit system with respect to the beam axis. The cross section formula developed above was applied to the laboratory coordinate system. It is convenient, however, for the interpretation of the cross section data to refer the scattering process to the coordinate system in which the center of mass of the proton-helium system is at rest. In the laboratory system, of course, the center of mass is moving and it has a velocity one-fifth that of the incident proton. In the center-of-mass system the proton and helium nucleus are moving toward each

other. In general, we find that in the conversion from the laboratory coordinate system to the center of mass coordinate system one must convert angles, energies and intensities.

Center-of-Mass Angle:

$$\Omega = \theta + \delta ,$$

where θ = laboratory angle and

$$\delta = \mathrm{Sin}^{-1} (1/4 \ \mathrm{Sin}\theta) .$$

Intensity Ratio.

The relative intensities of the scattered particles in the two coordinate systems are inversaly proportional to the elements of solid angle in the two systems.

Thus $$I(\Omega) 2\pi \sin\Omega \, d\Omega = I(\theta) \, 2\pi \sin\theta d\theta ,$$

and $$\frac{I(\Omega)}{I(\theta)} = \frac{\sin\theta}{\sin\Omega} \frac{d\theta}{d\Omega} .$$

The evaluation of this ratio gives

$$\frac{I(\Omega)}{I(\theta)} = \frac{4/25 \sqrt{16-\sin^2\theta}}{E_p/E_o} , \qquad (2)$$

where E_p is the scattered proton energy in the laboratory system and E_o is the incident proton energy.

Energy Ratio:

$$\frac{E_p}{E_o} = \frac{1}{25} \left(\cos\theta \pm \sqrt{16 - \sin^2\theta}\right)^2 . \qquad (3)$$

In the particular process under consideration the incident nucleus is lighter than the target nucleus and, hence, it is scattered with a single discrete energy in an elastic encounter. Thus, only one sign is used and this is the plus sign. To see this, consider the equation as $\theta \longrightarrow 0$, for which $E_1 = E_o$. For $\theta = 0$, the bracket term becomes 1 ± 4 and, hence, for $E_1 = E_o$ only the positive sign can be used.

Equations 1, 2, and 3 were used in converting the cross section values from laboratory coordinates to the center-of-mass system. Certain features of the transformations may be seen from inspection of these fundamental relations. First of all, the center-of-mass angles do not differ greatly from the laboratory angles. The maximum difference is of order of 14 degrees at $\theta = 90$ degrees. This might be compared with the case of proton-proton scattering where Ω (CM) = 2 θ (LAB). Secondly, the intensity ratio varies essentially inversely as the scattered particle energy. The ratio increases by a factor of 2 to 3 in passing from the forward angles to the backward angles.

With regard to the recoil helium nuclei from the scattering process, one finds as expected from the mechanics that these will have zero energy at 90 degrees and a maximum energy of 0.64 E_o at zero degrees. The expression for the recoil helium energy is

$$\frac{E_2}{E_o} = \frac{16}{25} \cos^2 \phi \ .$$

If one considers the emulsion equivalent of the gas in the chamber and

uses the recent range energy data of Rotblat[10], the expected range of the helium nuclei in the emulsion turns out to be approximately four microns at 50 degrees. The plate at this angle showed the short heavy tracks corresponding to these recoil nuclei. At slightly higher angles the range is too short to be useable and above 60 degrees, the recoil particles were absorbed by the gas. At smaller angles a definite peak was obtained at the shorter range. This is shown in Fig. 12 (page 42) which is a histogram plot of the number of tracks vs. track length at 20 degrees. In Fig. 13 (page 43), the same plot for 150 degrees, it will be noted that the peak at the shorter range is not present, except for a few tracks due probably to slit scattering.

---

10 J. Rotblat - Nature 167, 550 (1951).

CHAPTER III

APPARATUS

1. General Arrangement - Beam Snout.

The scattering chamber or multiplate camera that was used in this experiment was developed at the Los Alamos Laboratories[11] for studying the angular distribution of the products of nuclear reactions and nuclear scattering. In order that a series of experiments could be conducted with this equipment on the 60" Cyclotron in Crocker Laboratory, the beam had to be brought out so that the scattering chamber would be in a field free region. However, the unshielded beam curves around and remains within the strong fringing field from the cyclotron. Thus, it was necessary to shield the beam from this magnetic field. An iron snout was constructed to bring the beam out to clear the magnet yoke. Fig. 2 shows schematically the general arrangement of the scattering chamber and beam snout in its relation to the cyclotron.

The beam snout was designed to reduce the magnetic field through which the beam passes to a sufficiently low value that it would clear the magnet yoke and could be centered on the scattering chamber. The snout was tapered, as shown in the figure, to reduce the scattering of the beam from the sides as it spreads out. At the cyclotron beam-exit-port, a water cooled collimating slot was provided with dimensions of 1/2" x 1-1/4". (The beam cross-section at this point is approximately 1/4" x 1-1/2"). The inside dimensions of the snout tapered from these

---

[11] J. C. Allred, et. al., (See Ref. 7)

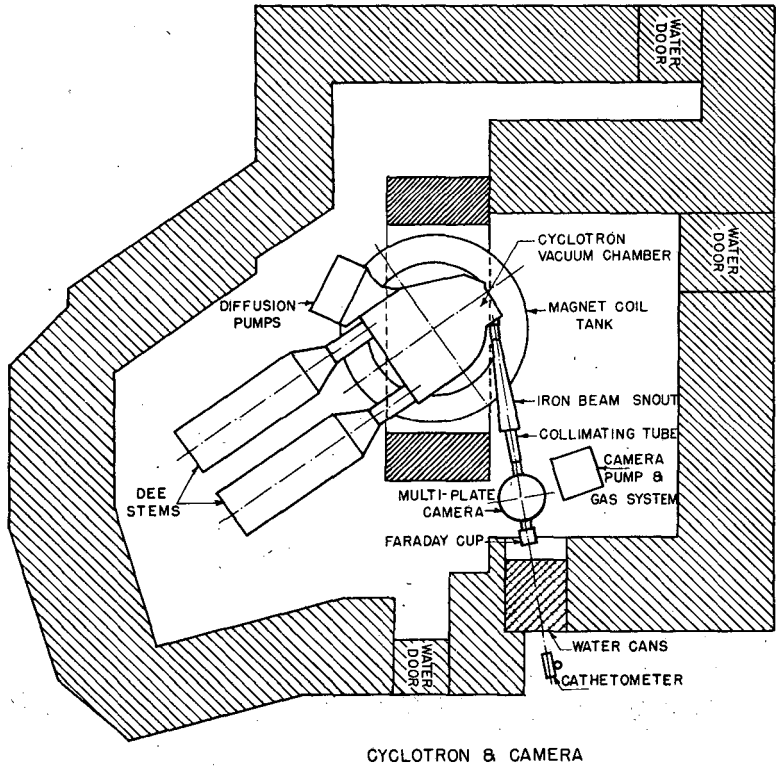

CYCLOTRON & CAMERA
SCHEMATIC

Figure 2

MU 2269

dimensions to 1-1/2" x 3" at the exit end, a distance of approximately 5 feet. In addition, a sylphon section at the cyclotron end allowed for adjustment to center the beam on the exit end. The snout was fabricated with cold-rolled steel and welded to make a vacuum tight chamber. The top and bottom were 5/16" thick and the side pieces 1-1/2" wide. With this amount of iron the field at the input end was reduced from 9000 oersteds to approximately 800 oersteds as measured with a portable G.E. flux meter.

At the exit end of the snout a second collimating slot was placed with dimensions of 1/2" x 3/4 inch. The connection from the snout to the scattering chamber was made by a brass pipe and sylphon bellows section with approximately 3 inches inside diameter. (See Fig. 3 for a general picture of the cyclotron snout and camera). An aluminum window, 0.001" thick (approximately 7 mg/cm^2) separated the scattering chamber from the cyclotron vacuum. The beam of approximately 20 Mev molecular hydrogen particles from the cyclotron, in passing through this foil, was converted to protons of approximately 9.5 Mev energy. The beam of protons then passed through additional collimating slits (or diaphragms) and, after passing through the scattering volume, entered a Faraday cup through a second window.

2. Scattering Chamber.

The scattering chamber has been described recently in the literature in its use in similar experiments to the present one.[12,13]

---

12 L. Rosen and J. C. Allred, Phys. Rev. 82, 777 (1951).

13 L. Rosen, F. K. Tallmadge, and J. H. Williams, Phys. Rev. 76, 1283 (1949).

Fig. 3

CYCLOTRON, SNOUT AND CAMERA LAYOUT.

The beam passes from right to left. The camera, pump and gas handling system are shown on the left.

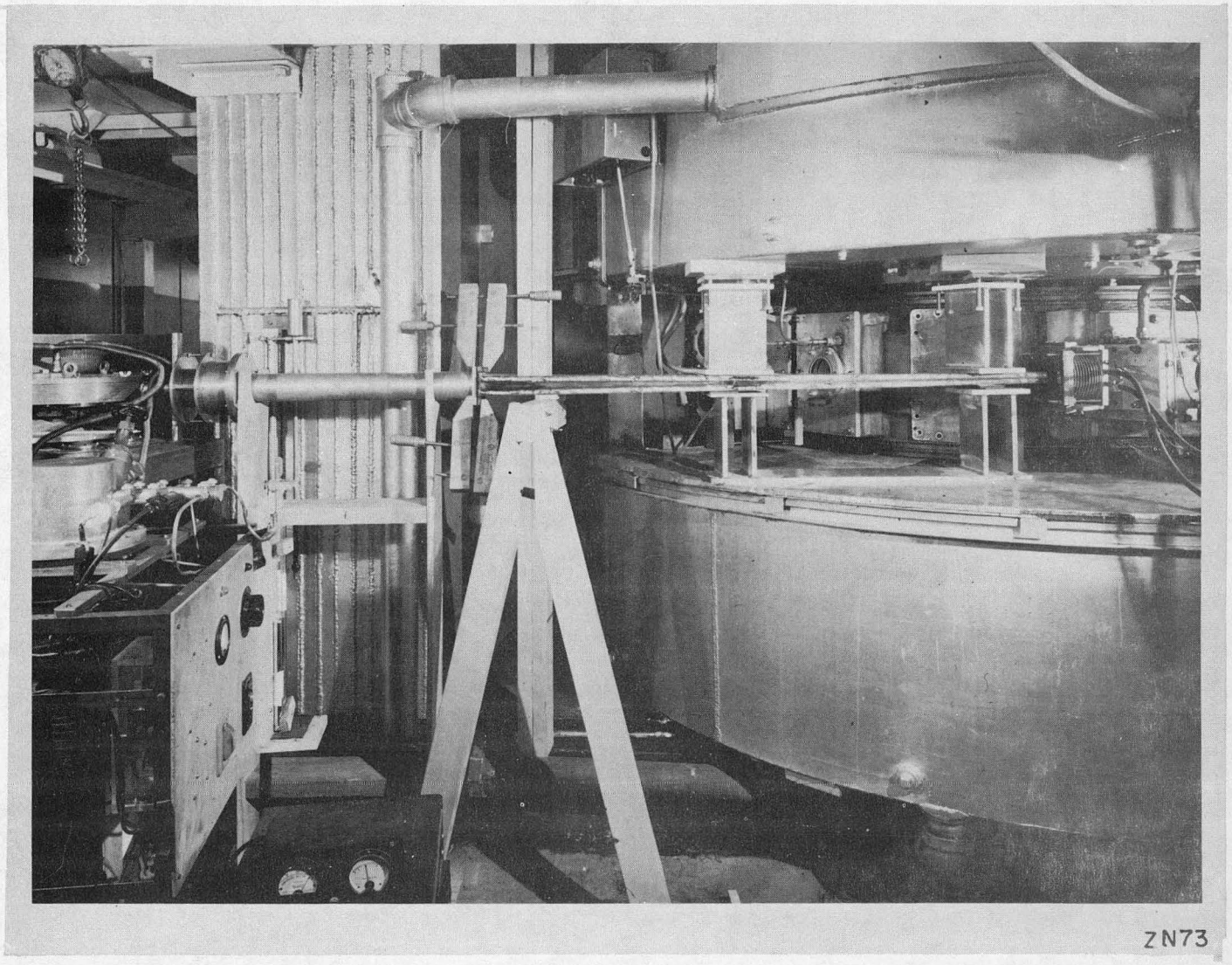

Fig. 3

However, since many of its features are of fundamental importance to the present experiment, a brief description will be given here.

The scattering chamber, or multiplate camera, is so constructed that every 2.5° angle from 10° to 172.5° can be monitored by means of a 1" x 3" nuclear emulsion plate. Fig. 4 shows, in schematic representation, the general arrangement of the multiplate camera. Sixty nine angles in all are covered and some of the forward ones twice. The beam of particles passes centrally through the camera, after being collimated by a set of four circular diaphragms. The diaphragms are enclosed in a tube which separates the beam from the scattering volume. Looking along the beam, the dimensions of the diaphragms are 3/16", 1/4", 3/16" and 1/4" in diameter. The first diaphragm is made of gold to reduce the production of neutrons by the incident beam. The 1/4" diaphragms act as anti-scattering baffles to stop part of the beam that is scattered by the edge of the first and third slits. In order to prevent the beam from striking the walls as it leaves the chamber, the exit tube is larger in diameter than the entrance tube. This allows for the spread in the beam as it passes through the chamber.

The slit system for the collimation of the scattered particles consists of essentially three concentric rings. The first and third rings contain the collimating slits of width 0.045 inches. The second or center ring contains anti-scattering slits to stop particles scattered by the edges of the inner slit and to prevent "cross-fire" between adjacent slit systems. These slits are 0.055" in width. Also, "anti-cross-fire" baffles are provided between the second and third slit rings. These are parallel to the slit axis and essentially isolate the adjacent systems over this region.

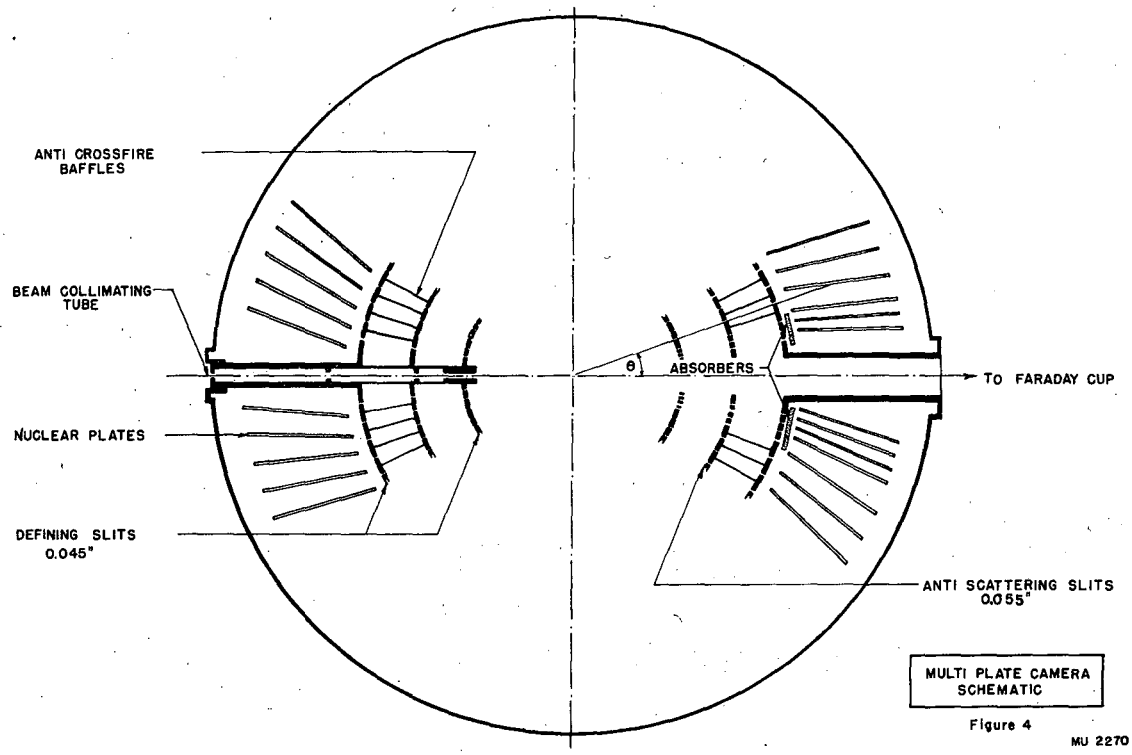

MULTI PLATE CAMERA SCHEMATIC

Figure 4

MU 2270

The nuclear emulsion plates, used to detect the scattered particles, are held in position between the outer slit ring and the wall of the scattering chamber. The position is such that the beam of scattered particles strikes the plate at a point about 3 cm. from its inside edge. A set of vertical slots holds the plate in position and beryllium copper springs on the outer wall insure that the inside edge of the plate is located against the outer slit ring assembly. The plates rest on the bottom of the chamber so that the exact location of the plate is determined and a reproducable geometry is obtained. In addition, slots are provided on each side of each slit in the outer ring assembly so that suitable foils may be inserted to slow down the scattered particle so that they will stop in the emulsion of the detector.

The angular spacing between the plates is 5° except at the forward angles. In this case three plates on one side and four on the other side of the beam axis have 2.5° spacing. With this arrangement the angles on one side are shifted by 2.5° from the angles on the other giving the 2.5° coverage for all angles from 10° to 172.5° as mentioned above.

Additional features of the multiplate camera which are of considerable importance in this type of experiment are:

(1) The defining slit rings fit into recesses in the camera lid and form a baffle which reduces the diffusion of water vapor from the emulsions into the scattering volume;

(2) The accuracy with which the camera slit system and plate holders were machined makes it possible to obtain results which have a relative accuracy essentially within the counting statistics for each angle. The camera was assembled with dowels and machined on

a special rotary dividing table capable of measurement with an accuracy of 10 seconds of arc. The estimated error in the angle between two plates is of the order of 0.1 percent which is negligible compared to the statistical accuracy usually used (1.5 - 2 percent).

There are several fundamental advantages in the construction and geometry used in the multiplate camera.

(1) Due to the accurate positioning of the plates, the geometry from one run to the next is exactly reproducible. This facilitates the comparison of data obtained on different runs.

(2) By using the two slit system, as shown in section II-1 above, the angle of the plate with respect to the slit axis does not enter into the cross section determination, eliminating any uncertainty in the measurement of the solid angle subtended by the detector.

(3) Of particular importance for obtaining the relative cross section is the fact that many plates (angles) can be exposed at one time providing a means of obtaining data under identical conditions for many angles. Also, being able to expose plates at many angles at one time shortens considerably the time required to obtain the data. This minimizes variations in beam position and beam energy from one run to the next over the duration of the experiment.

3. Pump and Gas Handling System.

Two separate pump systems were provided for evacuating the multiplate camera and the Faraday cup. The pump system for the Faraday cup consisted of a small air cooled oil diffusion pump and mechanical fore pump. A liquid air trap was used to trap condensible vapors and an ion gauge was provided for measuring the pressure. The

liquid air trap was kept filled at all times during the course of the experiment and the pressure in the Faraday cup unit was maintained in the range of 10^{-7} mm Hg.

For pumping down the multiplate camera, a 275 liter per second oil diffusion pump was provided and a mechanical fore pump was used for backing. Two sylphon pump lines connected the manifold to the camera. One line went to the scattering volume while the second line, which contained a liquid air trap, went to the annular region which contained the nuclear plates. This made it possible to pump out the two sections of the camera separately and to introduce the scattering gas directly with the liquid air trap isolated from the system. Fig. 5 is a schematic of the pump and gas handling system. By proper manipulation of the various valves provided, the multiplate camera could be pumped down, the liquid air trap could be closed off, and various roughing and finishing pumpdowns necessary for introducing the gas could be handled with ease. Both an ion gauge and a vacuum thermocouple gauge were provided for measuring the pressure. All small valves were Hoke sylphon needle valves while the large valves were 1" sylphon vacuum valves. The gate to the diffusion pump was a standard commercial diffusion pump gate valve. During the course of setting up the camera and pump system, the entire assembly was checked for leaks with a helium leak detector and made absolutely tight. Nominal values for the camera vacuum with plates in place were in the range of 10^{-5} - 10^{-6} mm Hg. The accepted rate of rise prior to a run was in the range of 6 - 10 microns/minute.

Key to Fig. 5

DP - Oil Diffusion Pump
FP - Mechanical Fore Pump
IG - Ion Gauge
HG M - Mercury Manometer
He GC - Helium Gas Cylinder
LA Trap - Liquid Air Trap
TCG - Vacuum Thermocouple Gauge

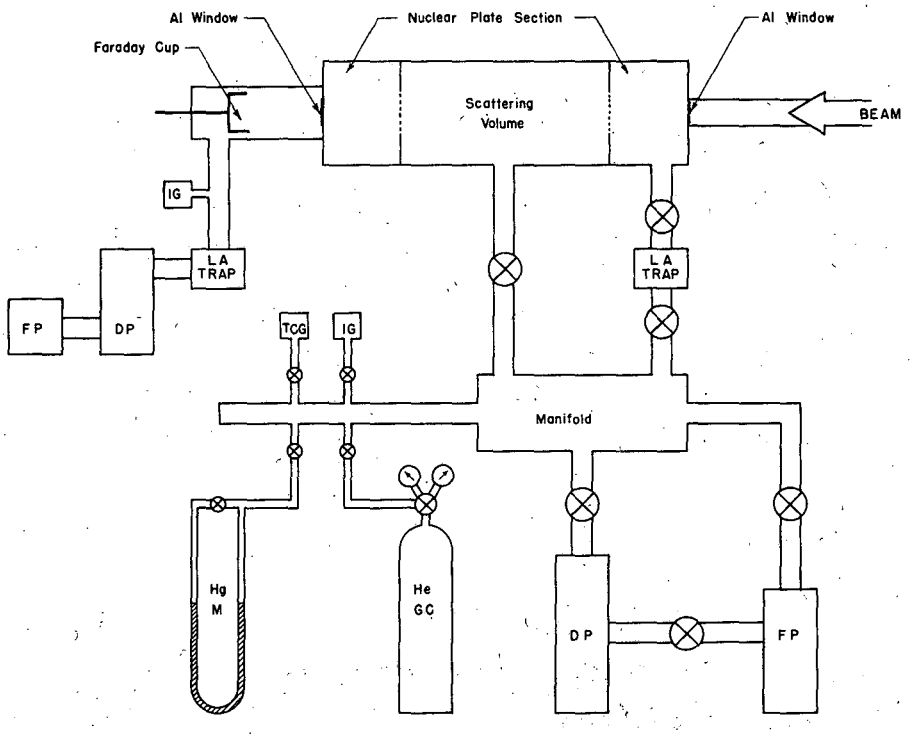

CAMERA PUMP and GAS SYSTEM
Figure 5

MU 2271

CHAPTER IV

NUCLEAR EMULSION TECHNIQUE

In recent years, with the development of improved methods for the preparation and handling of the special fine grain emulsions, the photographic plate has returned to widespread use in recording nuclear processes. The photographic plate was first used in 1896 by Becquerel when he discovered that the radiations from uranium salts were capable of blackening a plate. Later, when it was discovered that high speed alpha-particles in passing through an emulsion left a line of developable grains, the photographic plate was used by various workers to record nuclear events. However, this work was handicapped by the characteristics of the early photographic emulsions. Primarily, the emulsions were too thin to stop the incident particles and complete data was difficult to obtain. Secondly, the silver halide content of available emulsions was so low as to make it very difficult to distinguish an actual track since the silver grains were rather widely spaced. With the nuclear emulsions available today, these difficulties have been largely overcome and the photographic plate for recording nuclear events is now considered as a standard recording device in many varieties of experiments.

The history, development, theory, and use of the photographic plate in recording nuclear events have been treated quite extensively by Shapiro,[14] Webb,[15] Powell and Occhialini,[16] and Yagoda.[17]

---

14 M. M. Shapiro, Rev. Med. Phys. 13, 58 (1941).

15 J. H. Webb, Phys. Rev. 74, 511 (1948).

16 C. F. Powell and G. P. S. Occhialini, Nuclear Physics in Photographs, Oxford, (1947).

17 H. Yogoda, Radioactive Measurements with Nuclear Emulsions, Wiley, (1949).

The reader is referred to these references for detailed information concerning the nuclear emulsion technique. The discussion here will be limited to the specific application involved in the experiment.

Before proceeding with a discussion of the techniques used in the experiment, it might be well to briefly consider some of the advantages and disadvantages in the use of nuclear emulsion detectors for scattering experiments. First of all, the nuclear plate is continuously sensitive to charged particles. As such it will record all processes taking place in the scattering chamber during the run. This means that if, in addition to the elastic scattering process, another process takes place, any particles from this event which have sufficient energy to reach and enter the emulsion will be recorded. Secondly, because of its compact size, a great many plates can be used simultaneously as was done in this experiment. The obvious advantages of this feature have already been mentioned. The known position of the plate with respect to the scattering volume is still another advantage in that by use of suitable acceptance criteria, background and spurious particles can in general be eliminated in the counting. Finally, the auxiliary equipment needed with electronic counter type detectors, (e.g., power supplies, amplifiers, scalers, discriminators, and all the associated cables) is eliminated. Coupled with these advantages however, is the fact that the data is not immediately available due to the time required for plate development. In addition, the job of analyzing each plate is tedious and requires 20 to 25 hours for the type of analysis and number of tracks counted in this experiment. On the other hand, the data can be recorded on the plates and the analysis can be made at a later time. In the present experiment, much of the counting was done with the help of a single technician and the analysis of forty-seven plates required

approximately four months. Finally, the photographic plates provide a permanent record of the experiment.

The photographic emulsions used in the present experiment were 100 micron and 200 micron Ilford C_2 emulsions. These recorded the protons as a moderately dense track and the alpha-particles as a very dense track enabling these to be distinguished quite easily. The 200 micron emulsions were used only at the forward angles where the expected proton range was too long for protons to remain in the 100 micron emulsion. This was determined by the expected scattered energy and plate angle, which was 11 degrees 46 minutes for all scattering angles.

The procedure for handling the plates during the experiment will be discussed in the next chapter. Once the plates had been exposed, they were immediately removed from the vacuum and started through the developing process. The developing was done in an automatic machine built specially for developing nuclear plates by the Film Group of the Radiation Laboratory. The plates were put through the following process:

(1) 30 min in developer (D - 19 diluted 6 parts of water to 1 of stock)

(2) 12 min in running water, 68°

(3) 2 hrs. in Kodak acid Fixer with Hardner

(4) 2 hours in running water wash

(5) allowed to dry slowly.

No special precautions were taken to prevent peeling although the edges of some of the plates were taped with scotch tape. In the first trial run some plates a few months old were used and these peeled rather badly. However, on all succeeding runs, new plates (approximately one week old) were used and to date these are all in the same useable condition as when they were originally developed.

With the plates exposed and developed, the final process was that of analyzing the tracks recorded on the plate. Since the plate is continuously sensitive to all reactions taking place during exposure, each plate had to be very carefully analyzed to ensure that all possible data was noted and full advantage taken of the information available on the plate.

The microscopes and laboratory arrangement used for the analysis of the plates in this experiment are shown in Fig. 6. The microscopes were both Zeiss Jena laboratory binocular microscopes. The light sources were Bausch and Lomb research microscope illuminators with a ribbon type filament. These gave a uniform and intense source of light which made examination of the plates easier. Note the plexiglass dust covers used to protect the microscopes when they were not in use. Also each microscope and its illuminator was fixed on a common base so that the critical illumination used could not be jarred out of adjustment. The microscopes contained apochromatic objective lenses with compensated eye pieces. A sixty power objective and ten power eye pieces were used on all measurements. With an additional factor of 1.5 in the body tube, the total magnification was 900X.

A reticule consisting of a large ruled square subdivided into 100 sections engraved on an optical glass disc was used to define the swath width on each measurement. The reticule was placed in one of the eyepieces and the observer used only that portion of the field of view within the square in selecting the tracks that were counted. A stage micrometer and auxiliary eyepiece scale were used to calibrate the reticule.

In order to facilitate the measurement of the projected ranges of the tracks selected, a special superstage was devised for the micro-

FIG. 6

MICROSCOPE LABORATORY ARRANGEMENT.

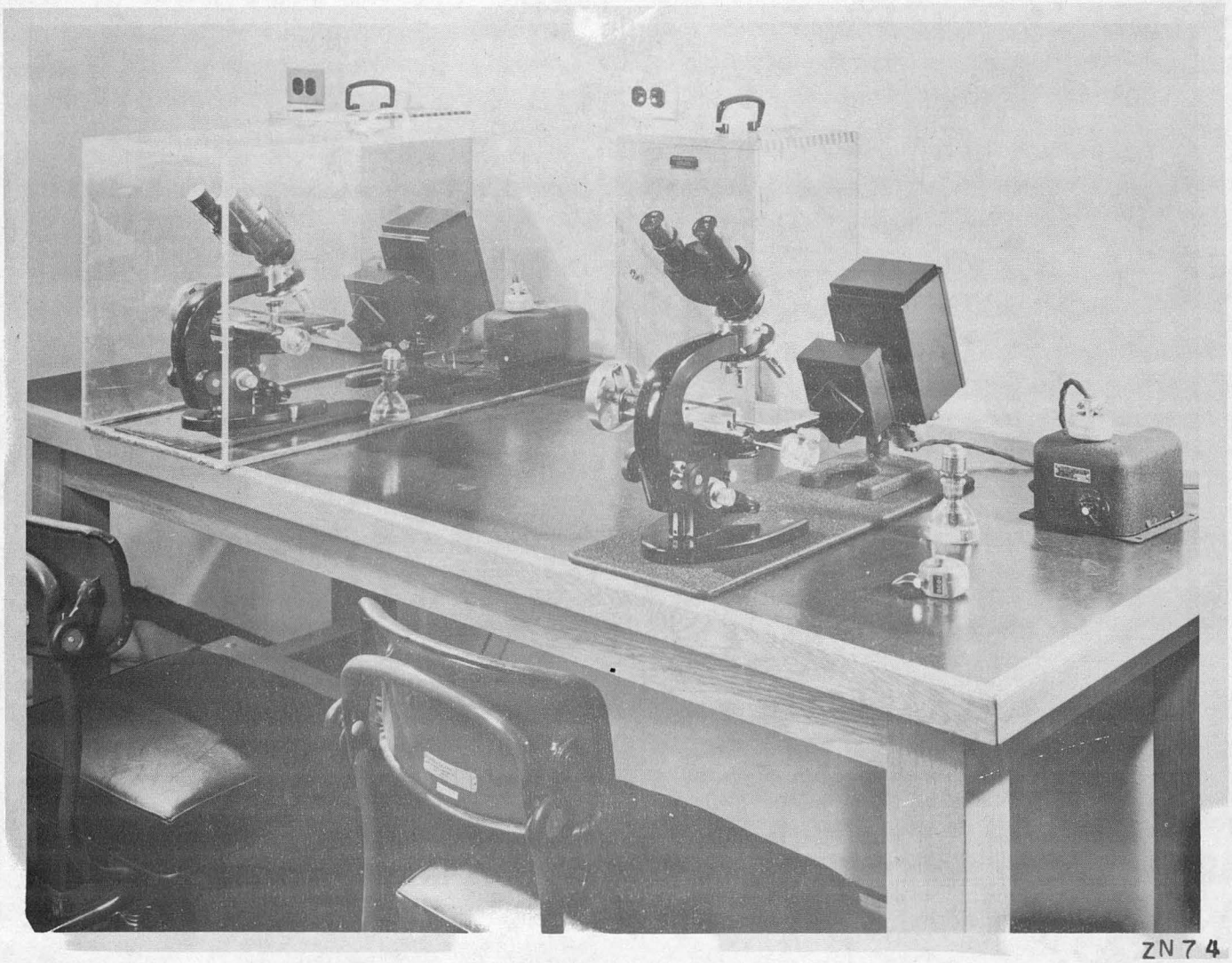

Fig. 6

scopes and two of these were fabricated by a local optical instrument company. The basic principle used in the design of this superstage was that the major portion of the tracks on the plate proceeded nearly parallel to one direction, that of the defining slit axis. Thus, precision measurements were needed, in general, only in one direction on the microscope. The construction of the superstage is shown in cross-section in Fig. 7 and photographs of the actual stage are shown in Figs. 8 and 9. The stage was designed to move the plate separately from the regular microscope cross feed screw. The traversing bar was located in the groove which normally holds the clamps for the plate-holder arms. By using this construction, the position of the plate-holder arms was unmodified with respect to the microscope stage and the relation of the photographic plate to the condenser substage was not altered. The superstage screw was a Zeiss precision screw of one-half millimeter pitch and the calibration on the drum was two microns per small division. With this stage precision, measurements in the horizontal direction could be made quickly and easily. The reproducibility and accuracy of this device was checked quite carefully and one micron accuracy was easily obtained. With this additional screw, the time for the scanning, measuring and counting procedures was reduced by a factor of from 3 to 4, and the overall accuracy of the measurements was increased considerably. An additional feature is that the microscope was not altered in any way except for the plate holder and could be returned to its original state in a matter of a few minutes. It should be noted that the design is not limited in its application to the Zeiss microscope but can probably be applied to every microscope commercially available today.

The criterion used in counting tracks was based primarily on the slit system geometry. From this geometry (see Fig. 1), it is easily

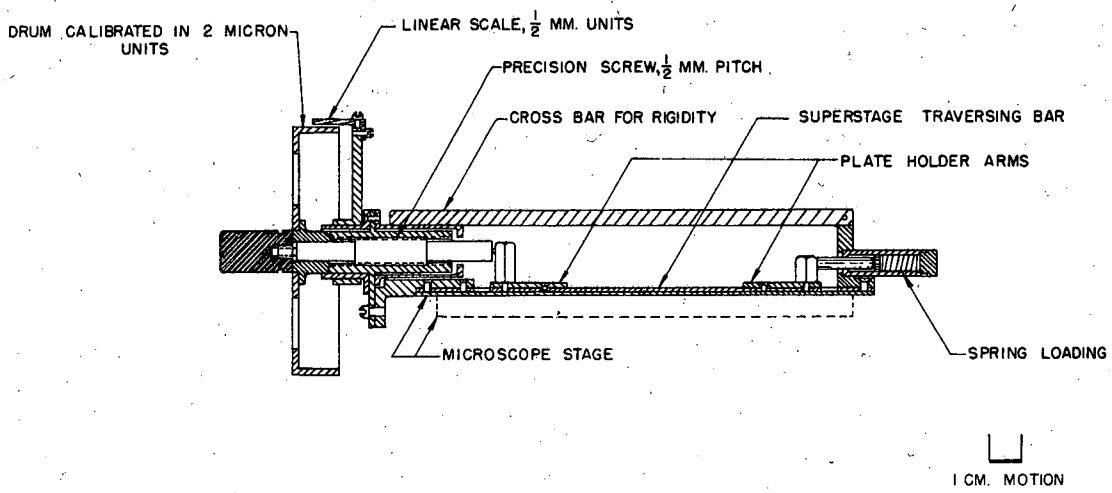

MICROSCOPE SUPERSTAGE

FIG. 7

MU 2272

FIG. 8

MICROSCOPE AND SUPERSTAGE.

Observers view.

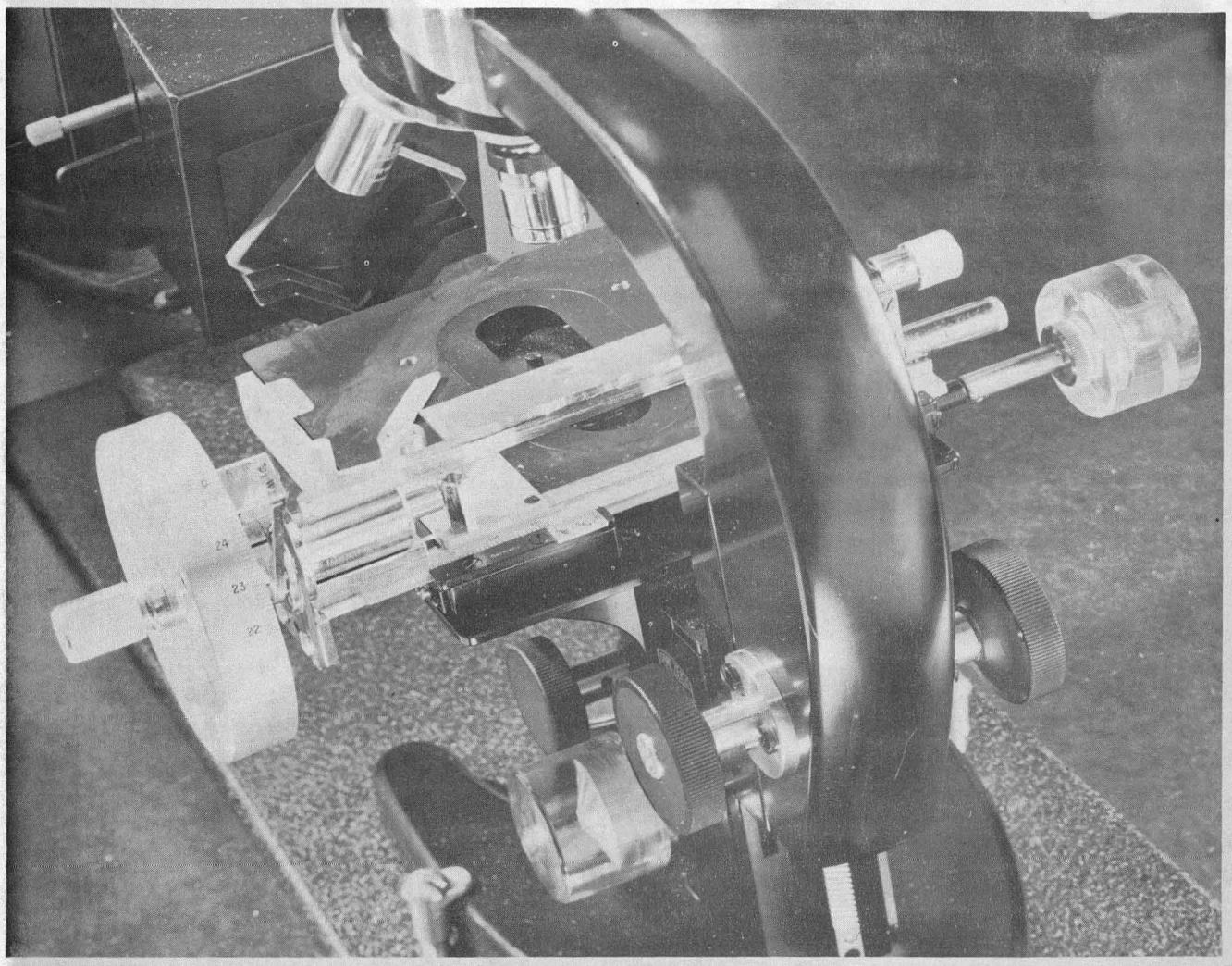

ZN 75

Fig. 8

Fig. 9.

MICROSCOPE AND SUPERSTAGE.

Light source side.

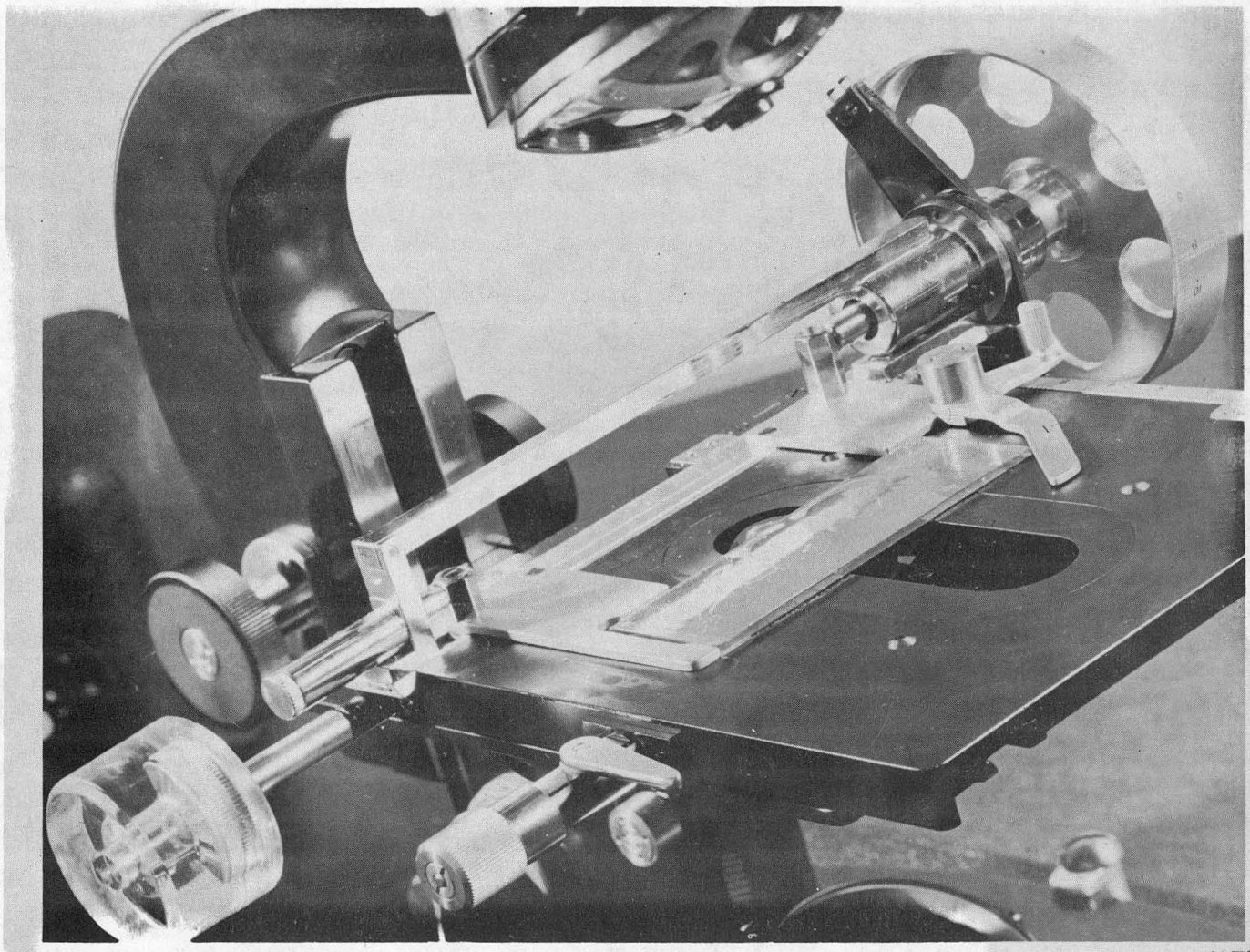

Fig. 9

seen that protons coming from a scattering event in the center of the chamber and passing through the slit system must enter the detector at the surface of the emulsion. In addition, they must proceed away from the inside edge of the plate and the direction of at least the first portion of the track must be within certain angular limits defined by the plate angle and slit geometry. Thus, by applying the proper angular limits and noting where the tracks start and the direction in which they pass, tracks could be selected which only come from the scattering volume. Further examination of the geometry will also show that the tracks will be found only over a narrow portion of the plate. The maximum number will occur at the axis of the plate slit system and the number of tracks will fall to zero on each side of this peak due to the angular resolution of the slits. Thus, by plotting the distribution of tracks on the plate, the position of the center of the distribution could be determined quite accurately. Since the inner edge of each plate was exactly positioned, the factor L which enters directly into the cross-section formula, could be accurately determined.

Figs. 10 and 11 are representative track density distributions on the plates at 20 degrees and 150 degrees. The main peak is reasonably symmetrical (within the statistics used) and covers actually only a small portion of the plate. The plates are approximately 75 millimeters in length and the tracks are located over only about 15 to 20 millimeters. The cross-hatched areas on the histogram represent tracks which fall outside the main range peak. (see below) At the forward angles the helium peak was considered as a main peak also. Thus, from the density distribution, one could be certain of including all of the tracks on the plate. In addition, at the forward angles where absorbers were used, the density distribution was used to determine whether or not all the

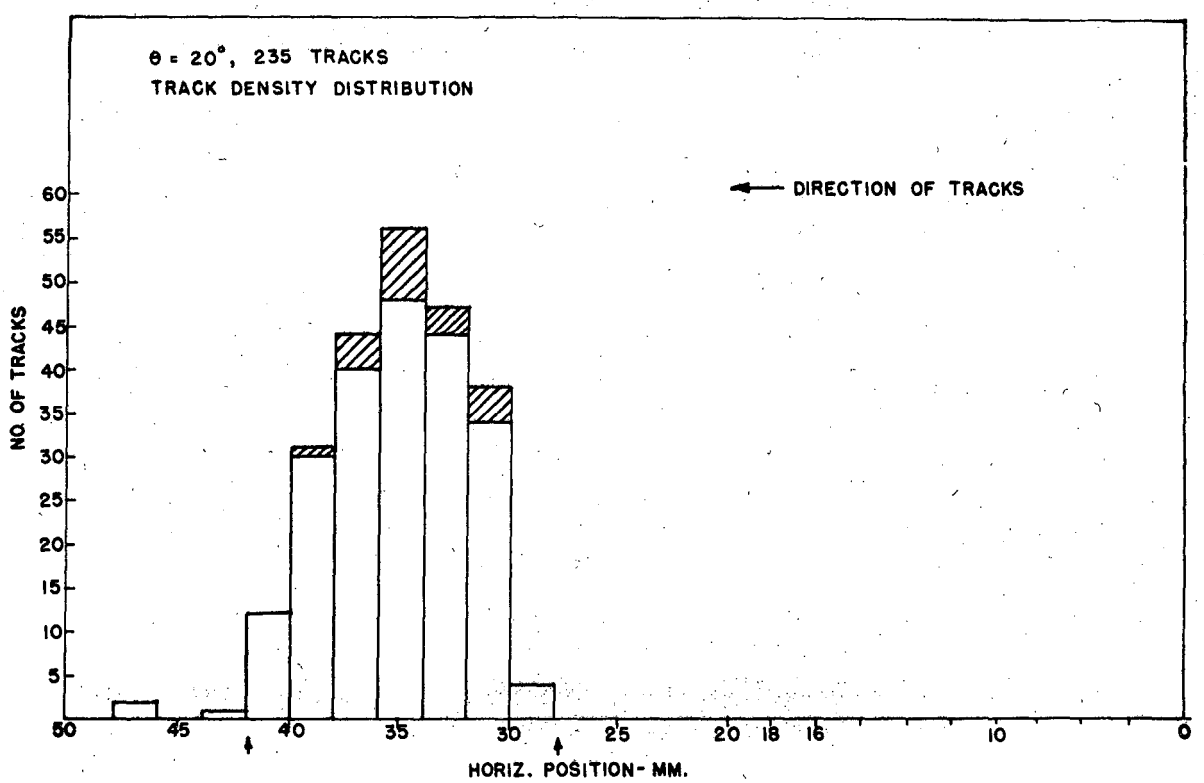

Figure 10

MU 2273

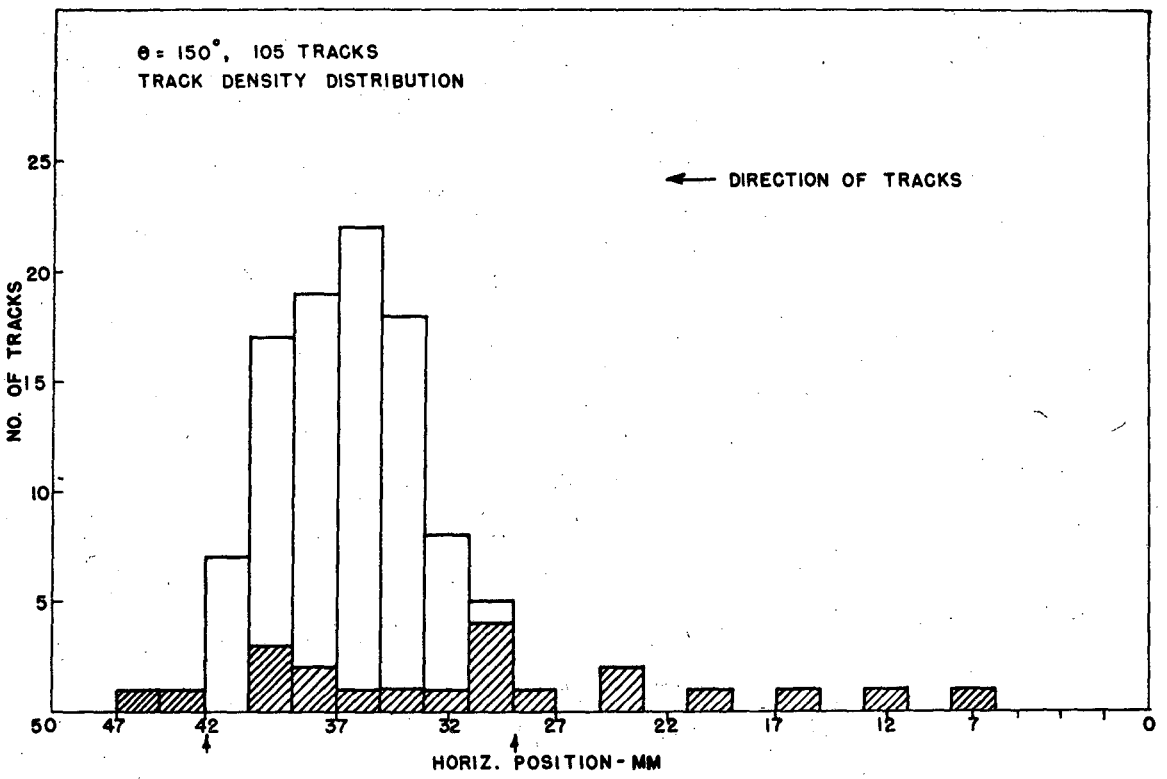

Figure 11

MU 2274

protons which passes through the slits entered the plate. This was found to be true although the distribution was spread over a much larger portion of the plate.

Since the approximate incident proton energy was known, then, from the mechanics of the collision, the expected proton energy at each angle was estimated. By making suitable allowances for gas absorption and plate angle, the mean expected range for the proton tracks from elastic scattering could then be determined. If a plot of the range of every track which satisfied the requirements above, is made for a few hundred tracks covering one or more complete swaths, this plot will indicate the actual distribution in proton ranges due to beam inhomogeniety and straggling. Such a plot will also indicate if any other process has taken place that will be observable on the plates. Figs. 12 and 13 are histograms of the range distributions for two angles, 20 degrees and 150 degrees. Note that at 20 degrees, two peaks were found. The shaded areas represent tracks which fall outside the main track distribution peak. As discussed in Section II-2, the long range peak is the desired proton peak and the shorter range peak is the expected peak for the recoil helium nuclei. It was from such plots for each angle that the incident proton energy for the experiment was determined (see Chapter VI).

The intermediate range peaks on these two histograms may be attributed primarily to slit scattered particles, that is particles which have penetrated the slits sufficiently to lose some of their initial energy. These particles by the nature of the defining system have not come from the allowed scattering region and, hence, are not counted. Also, from the small number of so called background tracks on the plates, the effect of neutrons produced in the defining slits by the incident

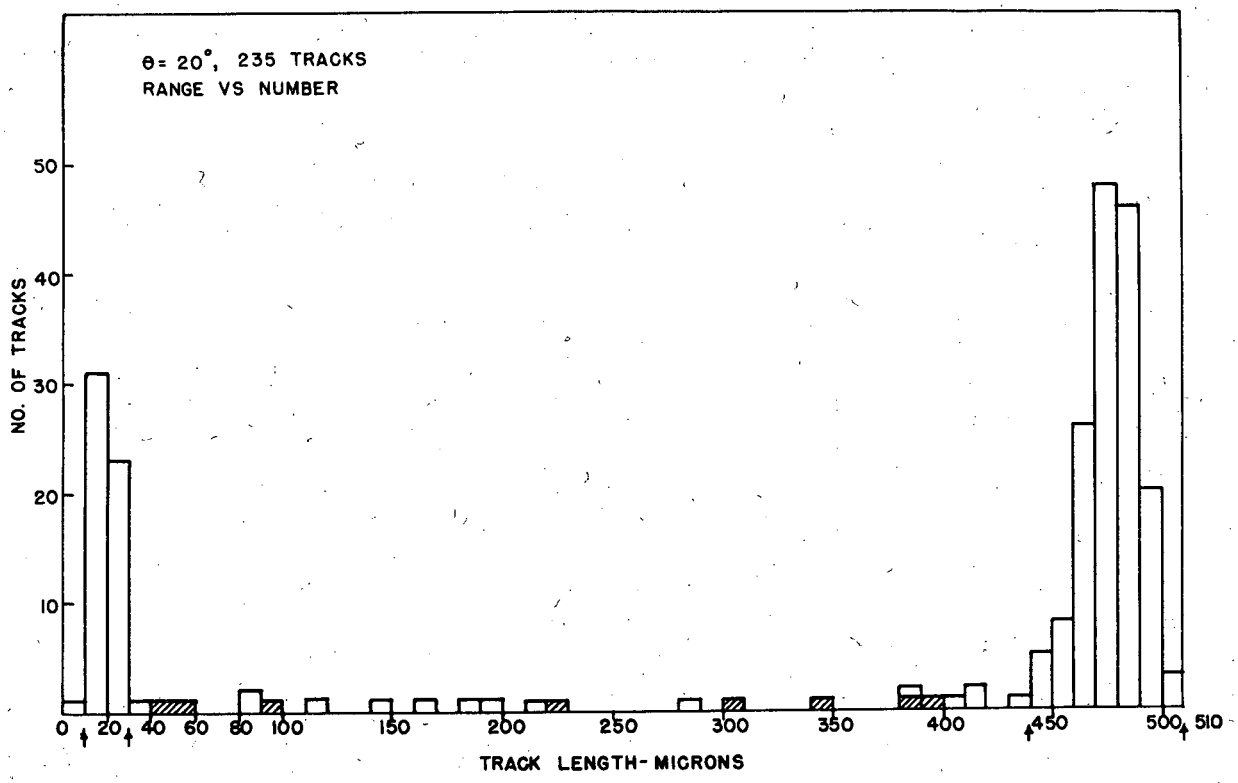

Figure 12

MU 2275

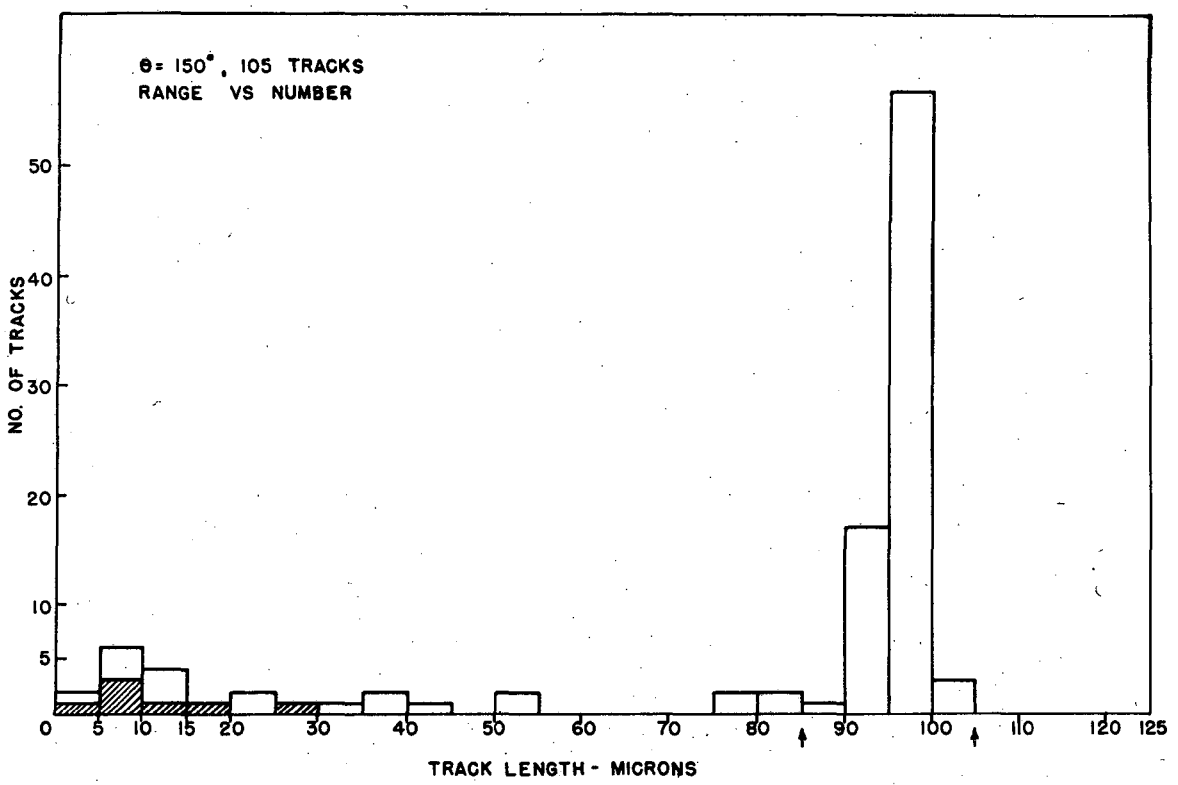

Figure 13

MU 2276

beam was apparantly negligibly small. Thus, by the proper use of the range distribution curve, the acceptance criterion as to range was determined eliminating most of the background and spurious track corrections. Based on the slit geometry and the range analysis for each plate, the following criteria were established for counting a track:

(1) The track must start on the surface of the elulsion.

(2) The track must proceed in the proper direction - this was specified by an index mark being placed on the inside edge of the plate. The track must proceed away from this edge.

(3) The track must enter the emulsion at such an angle as to have come from the scattering region. This, as determined from the geometry of the system, was a rectangular pyramid with angles of 7 degrees in the vertical plane and 12 degrees into the emulsion, i.e., in the horizontal plane.

(4) The track must have a range within the proton range distribution peak for the angle in question - the range limits were determined from the shape of the range peak.

(5) The track must enter emulsion within the field of view of the defining reticule.

With these criteria applied to each track, one is assured of obtaining accurate data. The limiting factor then will be the counting statistics. In the present work, a total of approximately 2500 tracks were counted at each angle. The actual number varied from this by one or two hundred due to the fact that complete swaths had to be read in accordance with the cross-section formula.

To summarize, the general procedure used in analyzing a plate was as follows:

1. All appropriate tracks (determined with the above criteria) in

one or more swaths were measured and their position noted in two millimeter intervals.

2. Range and density distribution histograms were then plotted. From these the acceptable range for counting tracks was determined. Also, the center of gravity of the density distribution and the mean range of the protons was determined.

3. With the range criterion together with the other acceptibility criteria, a sufficient number of swaths was counted to give approximately 2500 tracks.

4. Finally, a statistical plot was made of the number of tracks found in each swath and the number of tracks per centimeter swath width was calculated and drawn on the same graph. With this, the variation in number of tracks counted in each swath was easily checked. On those plates where the yield of tracks was low and many swaths had to be read, this comparison was used to determine whether swaths were being read which were too near to the edge of the plate and were falling outside the main track area. In the process of counting, each track had to be measured for its range. If the range fell inside the limits specified and the track satisfied the other acceptance criteria, it was counted. If, however, the range fell just outside the specified limits the range was noted on the data sheet. Also, if the track was much longer than specified, this range was also noted. By this method of recording the tracks one has a check as to whether all the valid tracks have been counted and as to whether impurity scattered particles have been included or not. A check of the energy of a few of these long tracks indicated they came from elastic scattering from nitrogen and oxygen (i.e., mass 14 and 16) nuclei. However, too few of these were observed to give good enough statistics to obtain even an estimate of the impurities present in the gas.

Thus, the value of Y, the number of tracks observed in a swath of known width was determined. The total swath width w was determined from the number of swaths read and the known width of the reticule. The ratio of these two numbers, Y/w, enters directly into the calculations of the cross-section for that angle. Certain corrections must be made on the value of Y but these were all applied together with other corrections and are discussed in Chapter VII.

CHAPTER V.

EXPERIMENTAL PROCEDURE.

1. Camera and Snout Alignment.

The beam snout assembly, which was designed to bring the cyclotron beam out so that the scattering chamber could be located in a field free region, has already been described. The first step then in setting up the scattering chamber was to adjust the final snout position so that the beam was centered on the outer collimating slot. This was accomplished by the use of a layer of zinc sulfide placed on a one-half inch thick glass port and fastened to the snout. The position of the beam was then observed on the plate from outside the water shielding and no over-exposure to radiation resulted. When the beam was approximately centered in the snout, a cathetometer was set up so that it pointed directly along the axis of the snout (see Fig. 2). The brass connecting section was installed and a second beam pattern was taken. Both the cathetometer and the snout were then re-adjusted to line up with this third point. The alignment of the cathetometer was checked by focusing on the last beam point, then on the exit slot of the snout, and then on the entrance slot of the snout (a distance of some 15 feet). When the cathetometer telescope was coaxial with these three points, the scattering chamber was installed and lined up along the same axis. From the appearance of the data, this alignment was good to better than 0.2 degrees.

Once the camera and Faraday cup were set up and satisfactorily aligned, the next step was to make the system vacuum tight. A helium leak detector was used and the only leaks of any consequence were found in the Hoke sylphon needle valves. Several of these were replaced before a complete set was found to be tight.

A further check of the magnetic field was made in the region of the scattering chamber. Rough measurements indicated an average field of the order of 70 oersteds at that point. Thus, although the chamber was perhaps 8 feet from the cyclotron beam port, it was still too close to the magnet to be in a low enough field for the proposed experiments. A one-half inch thick iron shield was finally installed on the sides with one-quarter inch on the top. This reduced the field to the order of 8 to 10 oersteds. For a 7-Mev proton in a 10 oersted gield, the radius of curvature is 15×10^3 inches. The length of path from the center of the scattering volume to the plate center is about 8 inches. This means that, the shift in the path of such particles at the plate, will be of the order of four thousandths of an inch which is equivalent of about two minutes of arc. However, the misalignment of the chamber was found to be of the order of 0.2 degrees or 12 minutes, i.e., six times the effect due to the small field present. Therefore, no appreciable error was introduced by this small field.

Fig. 14 is a close-up view of the scattering chamber showing a section of the iron shield. The chain rig shown hooked to the lid of the camera was used in removing the lid for loading and unloading the plates.

2. Handling the Nuclear Plates.

In order that the photographic plates (Ilford C2) could be loaded into the camera in complete darkness, the entire cyclotron area inside the water tanks was sealed off to make it light tight. This included sealing all the cracks between the water tanks and around the water doors. The nuclear plates were marked with their respective run number and position in the dark room. This mark was scratched into the glass on the back of the plate near one end. The plates were then transferred

Fig. 14.

MULTI PLATE CAMERA - S. SIDE.

The photograph shows a section of the magnetic shield and the camera lid lifting rig. The beam enters from the left. The Faraday cup, pump and ion gauge are on the right.

Fig. 14

in a light tight box to the cyclotron area and loaded into the proper positions in the camera. This process involved setting the plate in at the proper angle with the proper orientation (i.e., numbered edge against the inside slit ring and emulsion on the proper side to receive the scattered particles). The plates also had to be flush on the bottom of the chamber.

In Figs 15 and 16 the general arrangement of the plates in the scattering chamber is shown. In Fig. 15 the beam passes from the top to bottom of the picture. It will be noticed that the beam input tube is somewhat smaller than the exit tube and that both of these extend to the central region. The plate spacing is 5 degrees except at the most forward angles where 2.5 degrees spacing is used. The plate holder slots and energy absorber slots are also clearly visible. In Fig. 16, a photograph taken above but somewhat to the side of the camera, the defining slits for the scattered particles are clearly shown. On the top side of this picture (along the far edge of the chamber) the beryllium-copper springs which hold the plates into position against the inside slit ring assembly are also visible.

A rather extensive pumpdown time was required after the camera was loaded, due to the water vapor in the photographic emulsions. This period varied from four to six hours depending on the number of plates being exposed. The pumpdown procedure consisted in roughing down with the fore pump to a pressure of 100 microns and then pumping with the oil diffusion pump for the required period to outgas the plates. The liquid air trap, on the pump line to the annular area containing the plates (as shown in Fig. 5), was used during this period. The progress of the pumping was determined by taking a pressure rate of rise of the system with the liquid air trap closed off. When the rate of rise reached 5 to 10

Fig. 15.

MULTIPLATE CAMERA AND PLATES.

The beam enters at the top - the two sets of positioning slots are seen in the outer ring. The radial strips between the second and third slit rings are the anti-"cross-fire" baffles.

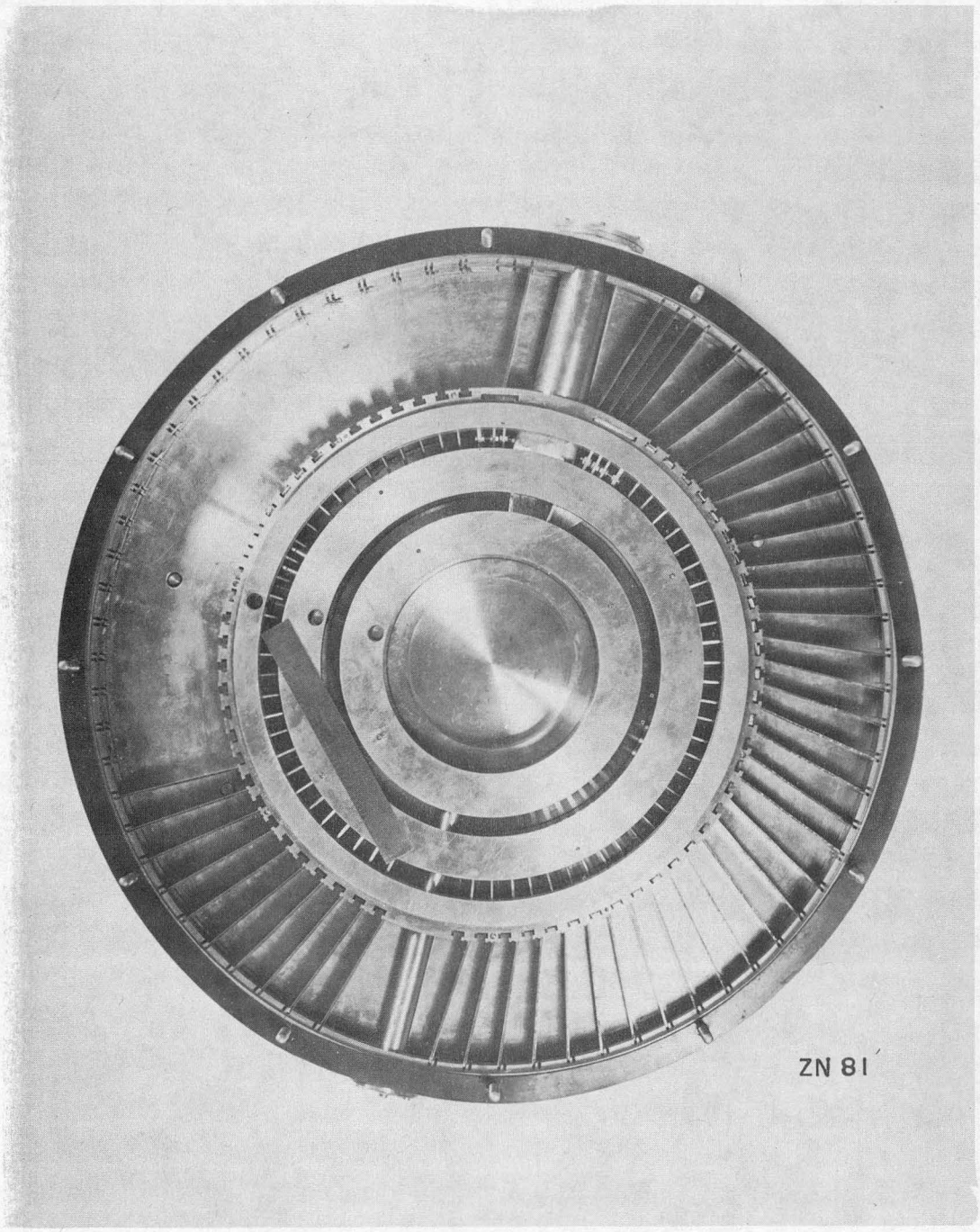

Fig. 15

Fig. 16.

THE MULTIPLATE CAMERA.

The inner and outer slit systems are shown together with the positioning slots for the plates. Also, the absorber slots are clearly visible in the foreground.

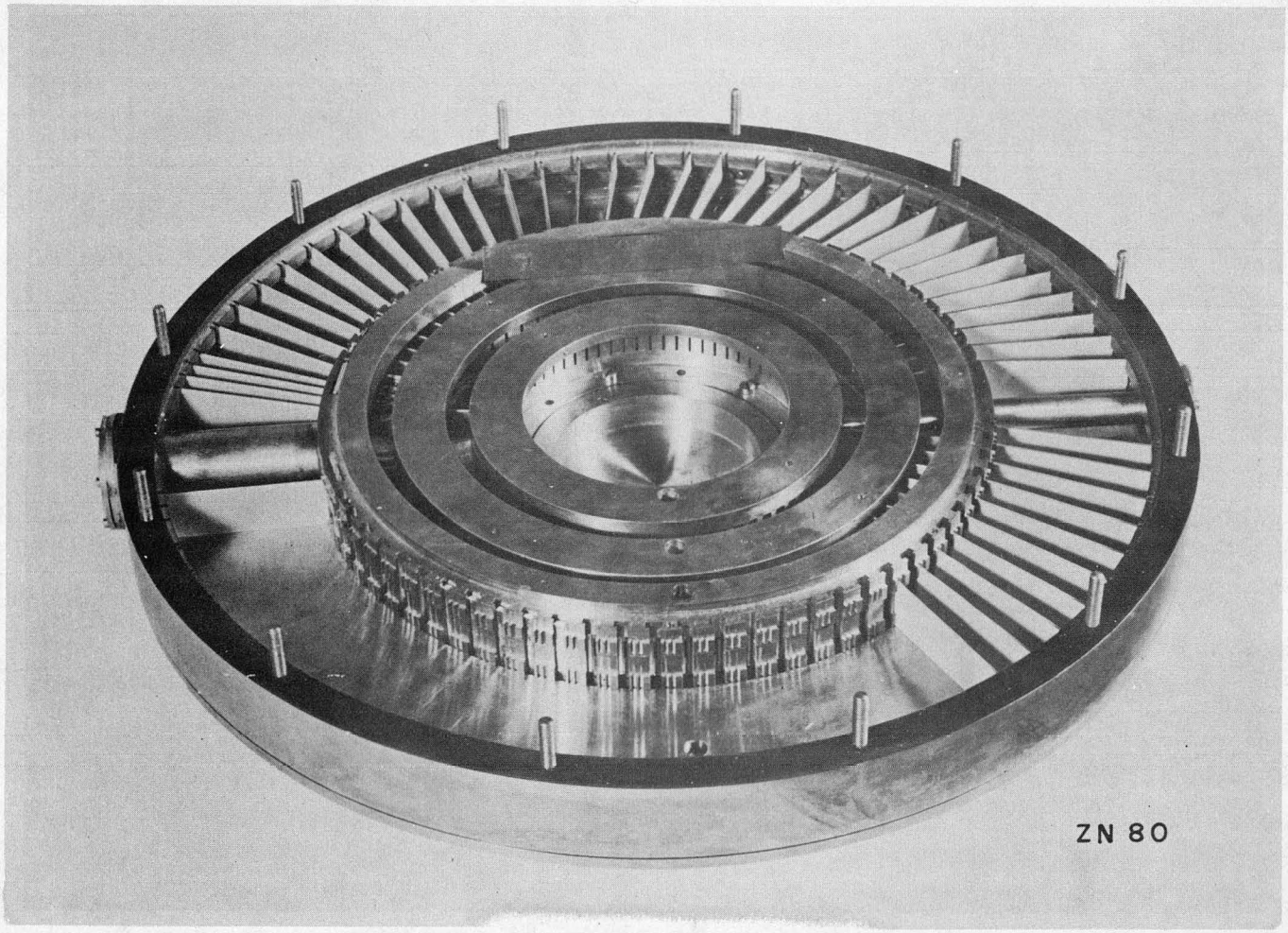

Fig. 16

microns per minute, preparations were made to inject the gas. The base pressure was usually in the neighborhood of 10^{-5} mm Hg at this point.

3. Gas Handling.

The procedure for admitting the helium gas to the system was quite straightforward. The system, including the regulator valve, had been previously vacuum checked as mentioned above. The entire gas system, manometer, gas lines and regulator system was pumped down to the base pressure, with the scattering chamber and liquid air trap cut off from the system. Both sides of the manometer were pumped down and the stopcock between these two arms was closed off. Then, with the diffusion pump gate and ion gauge valve closed, the manifold was opened to the chamber. Helium gas was then admitted directly from a commercial gas cylinder into the system to the desired pressure, as determined by the manometer. No effort was made to purify the helium since it was high grade gas. This type is double-charcoal purified, and has a rated purity of better than 99.9 percent. After an accurate pressure reading was taken, the manometer was closed off from the system.

The determination of n_o, the number of target nuclei per unit volume was based on measurements of the heights of the mercury columns in the manometer. A precision cathetometer was used for this measurement. The cathetometer was leveled and read by at least two observers. The temperature of the gas was taken as the temperature recorded by a thermometer placed directly under the chamber (see Fig. 17). Since the entire cyclotron area is enclosed by five foot water tanks, the ambient temperature remained fairly constant with only a slight rise noted due to the cyclotron magnet warming up during a run. The mean of the temperature readings before and after a run was taken as the temperature of the

gas during the run. The thermometer that was used was a 0° to $100^{o}C$ thermometer which was read to $\pm$ $0.1^{o}C$.

The relation used to calculate n_o is

$$n_o = k \frac{Pg}{P_o} \frac{T_o}{T_g} \frac{A}{V_s} ,$$

where n_o is the number of atoms per cubic centimeter, P_g is the pressure of the helium as measured above, P_o = 76 = standard atmospheric pressure in cm. of Hg , T_o = 273° Kelvin, T_g is the temperature of the gas, A is Avagadro's number and $V_s = 22.4 \times 10^3$ cm^3 = volume of a standard mole of gas. k = 1 = the number of atoms per molecule. Thus,

$$n_o = \frac{P_g}{76} \times \frac{273}{T_g} \times \frac{6.023 \times 10^{23}}{22.4 \times 10^3} = 0.9659 \times 10^{20} \frac{P_g}{T_g} .$$

The pressures used were in the range of five to forty centimeters of mercury (see appendix III). Corrections for the expansion of the mercury in the manometer, although small, were included in the final calculation.

The gas handling valves and manometer can be seen in Fig. 3. In Fig. 17 the general details of the camera and cup assembly are shown. The thermometer for measuring the gas temperatures is to the right under the camera. On the extreme right is the main liquid air trap. On the left is the Faraday cup and its electrostatic shield. Also, one of the Alnico bar magnets for the field on the cup is shown taped to the cup housing. The large sylphon tube connects the Faraday cup to its pump system. In Fig. 18 the position of the two flexible pump lines to the camera are visible. The line connected to the center of the chamber goes directly to the pump manifold. The other line, which is connected to the

Fig. 17.

THE MULTIPLATE CAMERA ASSEMBLY.

The Faraday cup and its electrostatic shield are on the left with the pump system below. The thermometer for measuring the gas temperature is located directly under the camera. On the right foreground is the liquid air trap.

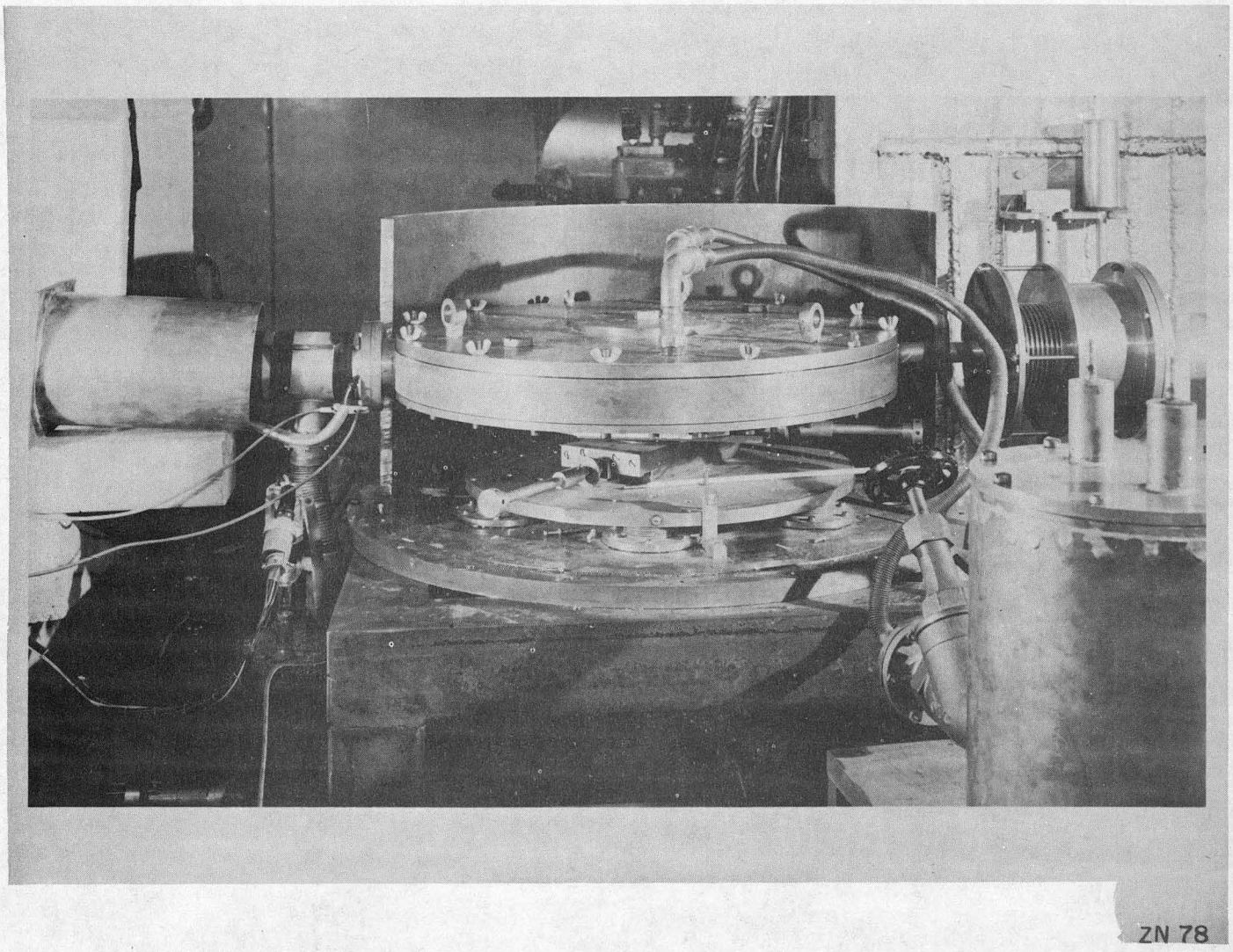

Fig. 17

Fig. 18.

THE MULTIPLATE CAMERA.

The Faraday cup and its electrostatic shield are shown on the left on the back of the camera. The positions of the two pump lines to the chamber are clearly visible.

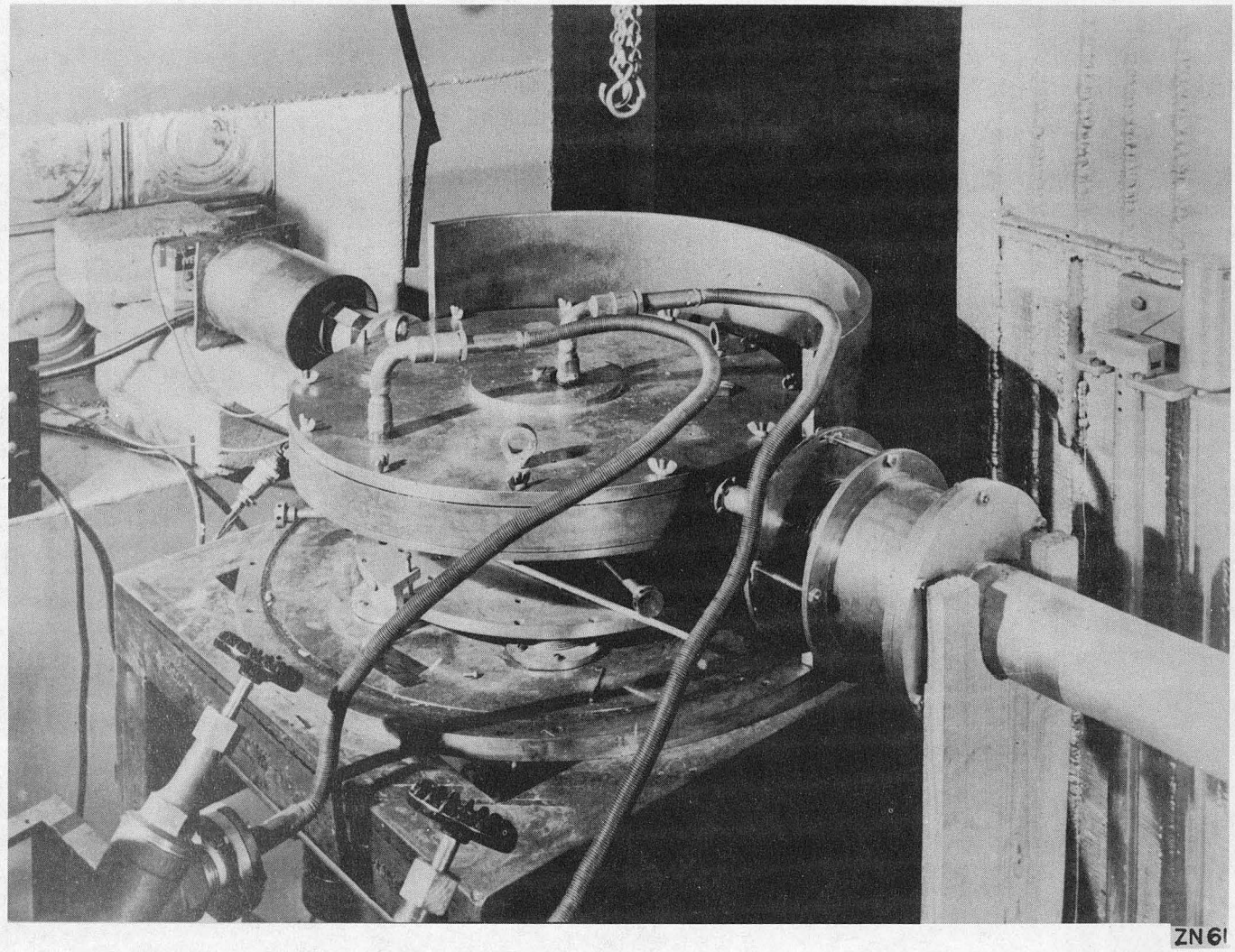

Fig. 18

nuclear plate section of the camera, goes to the liquid air trap and then to the pump manifold. In the foreground are the two main vacuum valves for the camera and in the background is the Faraday cup and its shield. The battery supplies the shield bias as is discussed below.

4. The Faraday Cup and Determination of N.

In order to obtain an accurate measurement of the total number of protons that pass through the chamber during a run and, hence, to determine N, a separate Faraday cup unit was provided. The Faraday cup itself was 9 inches in length and 1-3/4 inches in inside diameter. The cup chamber and pump system was fastened to the scattering chamber but separated from it by a thin (0.001 inch) aluminum window. Two Alnico permanent magnets were located above and below the cup so as to create a field of the order of 1000 oersteds. The purpose of this was to trap secondary electrons produced in the cup by the positive ions to prevent their escape. The Faraday cup was made negative with respect to ground by a battery placed in series with the lead to the current integrator. The purpose here was to prevent the collection of the electrons knocked out of the window by the beam.

The primary sources of leakage which would produce errors in the value of N were assumed to be:

(1) Ionization of the residual gas in the cup,

(2) Secondary electrons escaping from the cup,

(3) Conduction along the insulator surfaces.

As discussed above, the pressure in the Faraday cup was maintained in the range of 10^{-7} mm Hg. Thus, ionization of the residual gas should be a negligible factor, eliminating item (1). Also, conduction along the inner surface of the insulator would be essentially eliminated at this

pressure. To check for the possibility of secondary electrons escaping from the cup, the cup was made positive with respect to the case with a battery. A positive charge placed on the integration condenser was neutralized indicating negative integration. No integration was observed with zero potential on the cup. In the first case, secondary electrons from the surrounding surfaces were possibly the cause of this but it is more likely that it was due to leakage through the air as discussed below. The fact that no integration was observed when the cup was at zero potential indicates the effectiveness of the magnetic field in stopping secondary electrons from leaving the cup. In addition, the length of the cup and its large diameter together with the magnetic field provided to trap the electrons, gave added assurance that secondary electrons would not escape.

The only leakage point that needed correcting was the apparent conduction through the air and along the outside of the Faraday cup insulator. Since the experiment was performed inside the cyclotron water barrier, the radiation field (neutron and gamma ray) present when the beam was on was quite high. Various checks, that were made with different sized discs and wires hung on the integrator cable, indicated there was leakage due apparently to the ionization of the air by the radiation present. A further check of this effect was made with a one gram radium-beryllium neutron source. With the cable connected to the cup, the leakage rate was of the order of 65 micro-micro-coulombs per minute and with the cable disconnected, 9 micro-micro-coulombs per minute. The leakage rate also fell off inversely as the square of the distance between the source and the cup. This leakage was essentially eliminated by the use of an electrostatic shield placed over the cup and put at a

potential negative with respect to ground and of approximately the same value as that of the cup (see Fig. 19). This made the region around the cup and insulator essentially a field free region eliminating the leakage across the insulator. Leakage checks of the overall circuit with the various additions above, indicated a total leakage current of the order of 3×10^{-12} amperes. Hence, no corrections were made to N (the number of incident protons) for leakage in the integrating circuit.

Fig. 19 shows the general circuit used for integrating the current and Fig. 20 is a photograph of the current integration equipment. An accurately calibrated precision capacitor of 1.075 micro-farad capacity was used to integrate the charge. An electrometer and galvonometer circuit was used to indicate the voltage on the capacitor. The voltage was actually maintained at essentially zero by means of an associated slide-back voltmeter circuit. The procedure used was to maintain the voltage of the integrating condenser as near zero as possible by continually increasing the voltage from the slide-back voltmeter. The galvanometer was utilized to monitor the zero point voltage. At the end of a run the voltage on the slide-back voltmeter, which was required to completely and exactly neutralize the accumulated charge on the condenser, was measured with a Leeds and Northrup type K potentiometer and a General Radio type 654A decade voltage divider. A small drift in the electrometer was always present even with the capacitor discharged. A correction for this was applied by noting the zero drift at the end of each run.

The integrating capacitor was calibrated by means of comparison with a standard capacitor made commercially by the General Radio Company. This secondary standard was checked against the capacity of a Bureau of Standards calibrated condenser. The comparison was made with

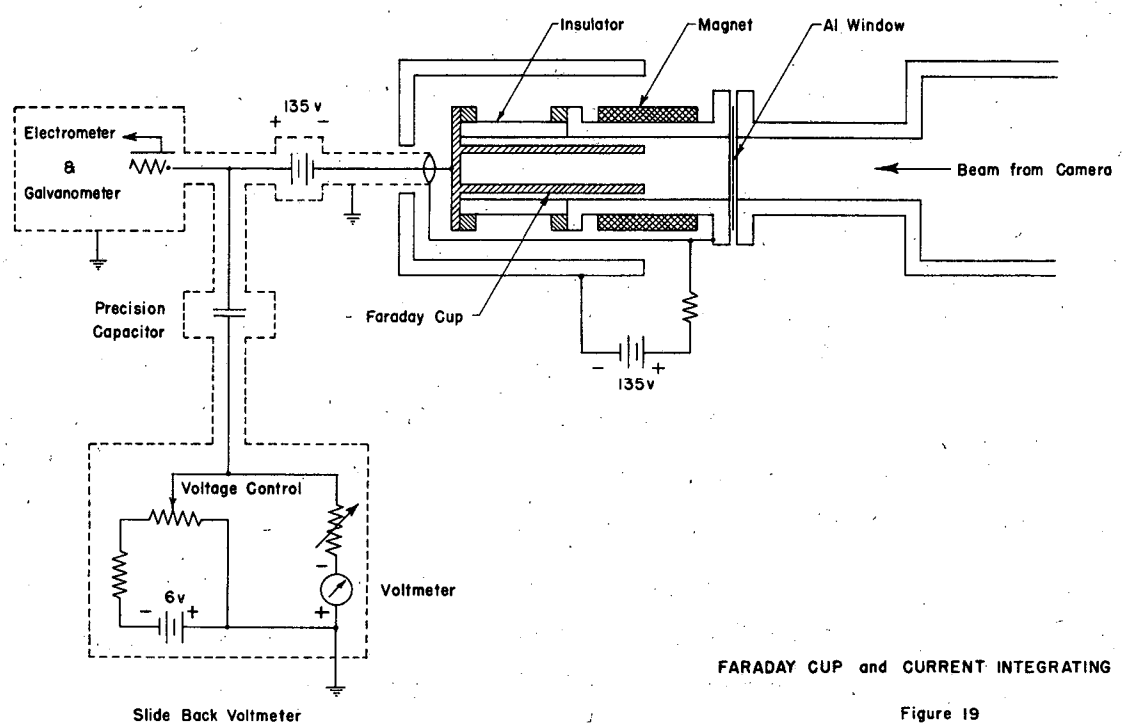

FARADAY CUP and CURRENT INTEGRATING CIRCUIT

Figure 19

MU 2277

Fig. 20.

CURRENT INTEGRATION EQUIPMENT

The potentiometer and galvanometer for measuring final voltage are on the left. The rack contains, in order, the galvanometer, electrometer and slide back voltmeter, condenser, and decade voltage divider.

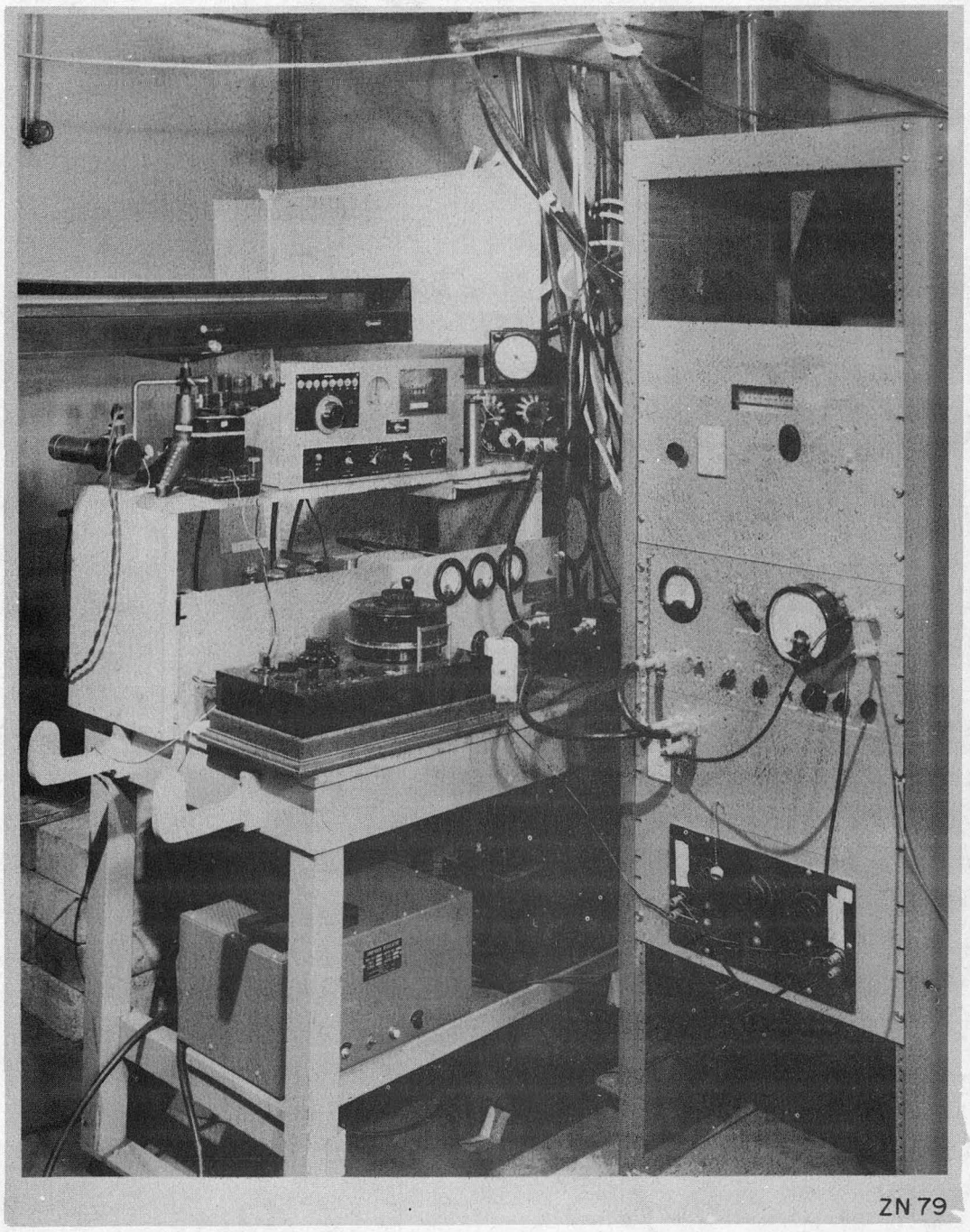

Fig. 20

a General Radio capacitance bridge by two different observers. The value given was 1.075 ± 0.005 micro-farads.

5. Exposure of Plates.

In the discussion above, the essential features of the procedures used for loading the nuclear plates, admitting the scattering gas, and determining n_o and N have been outlined. The exposure to be used for each run was determined from a preliminary run. In this run plates were exposed every 10 degrees at a pressure and current of 20 centimeters and 10 micro-coulombs respectively. Examination of these plates after development indicated the general exposure needed for various angles to take account of the large variation in cross section with angle.

A background run was also made to determine the presence of protons scattered from water vapor and other impurity gases other than those known to be present in the helium. This run was made following the same procedure used in handling the system for a regular exposure except that no helium gas was admitted. The use of this data will be discussed later.

CHAPTER VI

BEAM POSITION AND ENERGY

In principle, the beam position in the camera can be determined from the mean energies of the scattered particles at two angles, one on each side of the beam[18]. This is based primarily on the fact that, with the extreme care with which the camera defining slits were machined, the angle between two plates is known with great accuracy. Thus, if θ' represents the angle included between two slit systems on each side of the beam and θ is the unknown angle between the beam and one slit system, then this angle can be determined by the following method.

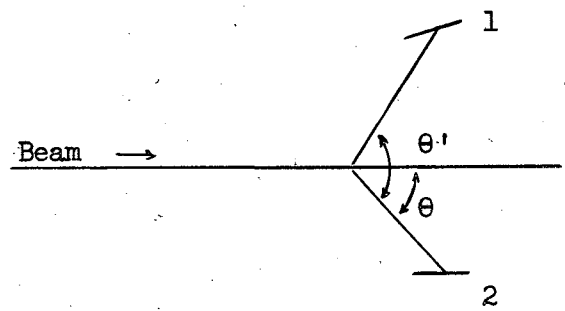

The mean ranges of the particles at the two angles are measured by the same observer under identical conditions. The plates used must, of course, be from the same run. From the range energy relation for nuclear emulsion, the beam energies can be determined. By applying suitable corrections for energy loss between the scattering center and the plate, the mean energies of the scattered particles can be obtained. From the scattering mechanics for the proton-helium case, we have

$$E_1/E_o = 1/25\ (\cos\theta + \sqrt{16 - \sin^2\theta})^2 ,$$

and for the two angle θ and $\theta'-\theta$ we can write

$$\frac{E_1}{E_2} = \frac{(\cos\theta + \sqrt{16 - \sin^2\theta})^2}{\left(\cos(\theta'-\theta) + \sqrt{16 - \sin^2(\theta'-\theta)}\right)^2} .$$

[18] L. Rosen, F. K. Tallmadge, and J. H. Williams, Phys. Rev. 76, 1283 (1949).

By solving this relation for θ as a function of E_1/E_2 and θ', the calculated value for the angle θ can be determined. The difference between this value and the specified value for the camera will give the true beam position. The solution of this gives a quadratic equation in tan θ of the form

$$K_1 \tan^2\theta + K_2 \tan\theta + K_3 = \theta ,$$

where

$$K_1 = \frac{15}{4}\left(\frac{R^2-1}{R}\right)^2 - \sin^2\theta', \quad R^2 = E_1/E_2 ,$$

$$K_2 = \frac{R^3+R}{R^2} \sin\theta' - 2\sin\theta'\cos\theta' ,$$

and

$$K_3 = \frac{R^3+R}{R^2} \cos\theta' + \frac{15}{4}\left(\frac{R^2-1}{R}\right)^2 - (1 \quad \cos^2\theta') .$$

The two possible solutions to this equation correspond to the case where plate #1 is on the one side or the opposite side of the beam. The particular value in question is easily determined by inspection.

Several sets of calculations were made using the above method and they all indicated a small error but the direction was not uniquely determined. The order of magnitude was fairly consistent, about $\pm$ 0.3 degrees. However, it was noted that the general trends in the direction of the error followed minor variations in the mean energy of the scattered particles as measured on the plates. This indicated that the above method was too sensitive to give a true indication of the beam position with the experimental accuracy available. By examination of the resulting cross section curve in the laboratory coordinate system, however, a definite trend was observed in the points on the two sides of the beam and a value of the beam position was determined graphically (see next section).

The determination of a value for the beam energy is somewhat more straightforward than the determination of the beam position. In fact, it is one of the advantages of the nuclear emulsion detector that particle energies may be determined with considerable accuracy. This means that the

beam energy can be determined from the scattered particle energies directly and there are no intervening windows requiring additional corrections. This method gives of course the average value of the energy during a run.

For the determination of the beam energy, the mean value of the proton range at each angle was obtained from the range distribution analysis. This gave the mean-projected-range on the surface of the emulsions. Corrections were made for plate angle and emulsion shrinkage in determining the absolute mean range of the protons in the emulsion and allowances were made for the energy loss in the gas between the scattering center and the plate. The energy loss in the gas was determined by calculating the emulsion equivalent of the gas and assuming that the emulsion equivalent of one centimeter of air is equivalent to five microns of emulsion at NTP. The emulsion equivalent of the gas for each run was calculated from the relations:

$$\frac{P_{targ}}{76} \cdot \frac{288}{T_{targ}} \cdot 5LS = \text{Emulsion equivalent in microns,}$$

where L = path length in the gas as determined from the center of gravity of the track density distribution on the plate. S is the stopping power of the gas with respect to that of air. This was determined over the energy interval in question from the range energy curves for protons in air and helium calculated by Aron, Hoffman and Williams[19]. The value used was 0.155 for the stopping power of helium relative to air for the energy range of three to nine Mev. The resulting values for the energy at each angle are given in Table C in Appendix III. The mean value of the energy from all the 47 plates was 9.48 ± 0.15 Mev.

[19] W. A. Aron, B. G. Hoffman, F. C. Williams, UCRL-121 (Revised) (1949).

CHAPTER VII

EXPERIMENTAL RESULTS

The results of the measurements of the angular distribution for the scattering of 9.5 Mev protons from helium are presented in two forms in the figures and tables of this section. The values for the differential cross section, corrected for background and impurity scattering, calculated with laboratory angles as measured from the central axis of the camera, are given in Table A. Examination of this data, particularly at the forward angles, indicates that the beam was not coaxial with the camera but was actually slightly off. For example, the relative accuracy of the data in any one run is essentially limited only by the statistics obtained in the counting. The values obtained from the plates at 10 degrees on each side of the beam should then be within 2 percent of each other. The actual difference obtained was approximately 18 percent. This difference is, of course, highly exaggerated by the sensitivity of the cross section to angle in the forward direction. The other forward angle plates, however, showed a difference which, although not as large , was in the same direction. Further, it should be noted that at the angles where overlapping data was obtained, the difference between the values obtained from two different runs for the same angle was well within the experimental accuracy. Examination of the full curve, for the relative positions of the points obtained from the two sides of the beam, also indicated a general trend in the position of these points in relation to the curve. By plotting the data from the two sides of the beam separately and placing one curve over the other, a uniform total shift of approximately 0.8 degrees in laboratory system made the two curves coincide within the statistical accuracy of the data. Due to the variation in cross section with sin θ, the actual shift necessary, as determined by this graphical method, was 0.4 degrees. Thus, all the angles

TABLE A

MEASURED CROSS SECTIONS AS A FUNCTION OF ANGLE IN THE CENTER-OF-MASS SYSTEM AT 9.48 MEV INCIDENT PARTICLE ENERGY

Cross Sections in barns, angles in degrees.

θ	Ω	dσ(Ω)/dω*				
		1	2	4	5	6
10.0	12.5		1.1597			
10.0	12.5		0.9701			
12.5	15.6		0.6703			
12.5	15.6		0.6192			
15.0	18.7		0.5414			
15.0	18.7		0.5022			
17.5	21.8		0.4817			0.4668
20.0	24.9		0.4093			0.3958
22.5	28.0					0.3812
25.0	31.1					0.3550
27.5	34.1					0.3408
30.0	37.2			0.3095		0.3055
32.5	40.2			0.3034		0.3118
35.0	43.2			0.2788		
40.0	49.3			0.2380		
42.5	52.1			0.2333		
50.0	61.0			0.1711		
52.5	63.9			0.1675		
60.0	72.5	0.1190				
67.5	80.9				0.0825	
70.0	83.6				0.0713	
72.5	86.3				0.0655	
80.0	94.2				0.0429	
85.0	99.4				0.0322	
90.0	104.5				0.0277	
92.5	107.0				0.0251	
97.5	111.8				0.02305	
100.0	114.2				0.02203	
102.5	116.6				0.02305	
110.0	123.6				0.0272	
115.0	128.1				0.0333	
120.0	132.5				0.0392	
122.5	134.7				0.0423	
130.0	141.0				0.0527	
135.0	145.2				0.0563	
140.0	149.25				0.0671	
142.5	151.25			0.0682		
150.0	157.2			0.0807		
152.5	159.1			0.0804		
160.0	164.9			0.0863		
162.5	166.8			0.0859		
170.0	172.5			0.0939		
172.5	174.4			0.0941		

* Data tabulated according to its run.

on one side of the beam were increased by 0.2 degrees and all the angles on the other side were decreased by this amount. The resulting data is plotted in Fig. 21 and tabulated in Table B. In the figure the data obtained from the two sides of the beam is distinguished by the open and shaded circles.

For the data at each angle approximately 2500 tracks were counted giving a standard deviation of ± 2 percent. The point at 60.2 degrees in laboratory system, however, was obtained from a plate exposed in the first or preliminary run. A preliminary analysis of this plate was made shortly after the run. Later the plate had peeled so badly that further tracks could not be counted with sufficient accuracy and so the preliminary count was used. Thus, only 547 tracks were counted for this point giving approximately ± 4.3 percent statistical accuracy.

In general, the internal consistency of the data for each run indicates an accuracy within the counting statistics. At the check points between runs, the differences are less than 3 percent, which gives an indication of the reproducibility of the experimental conditions from run to run, as well as giving some confidence in the absolute accuracy of the data. One region of the curve, however, shows an anomaly which has escaped an explanation. This is at the center-of-mass angles of 37.4 degrees and 40.0 degrees. The consecutive values of the cross section in run number six as shown by crosses on the curve in Fig. 21, are reversed in magnitude over the values expected from the general slope of the curve at this point. From the relative values of the overlapping data for these angles from run four and the shape of the curve at this point, it is very unlikely that any structure in the curve exists as indicated by this data. Repeated checks of the data and the associated calculations have failed to clear up this point. The anomaly in these two points is outside the 2 percent statistical

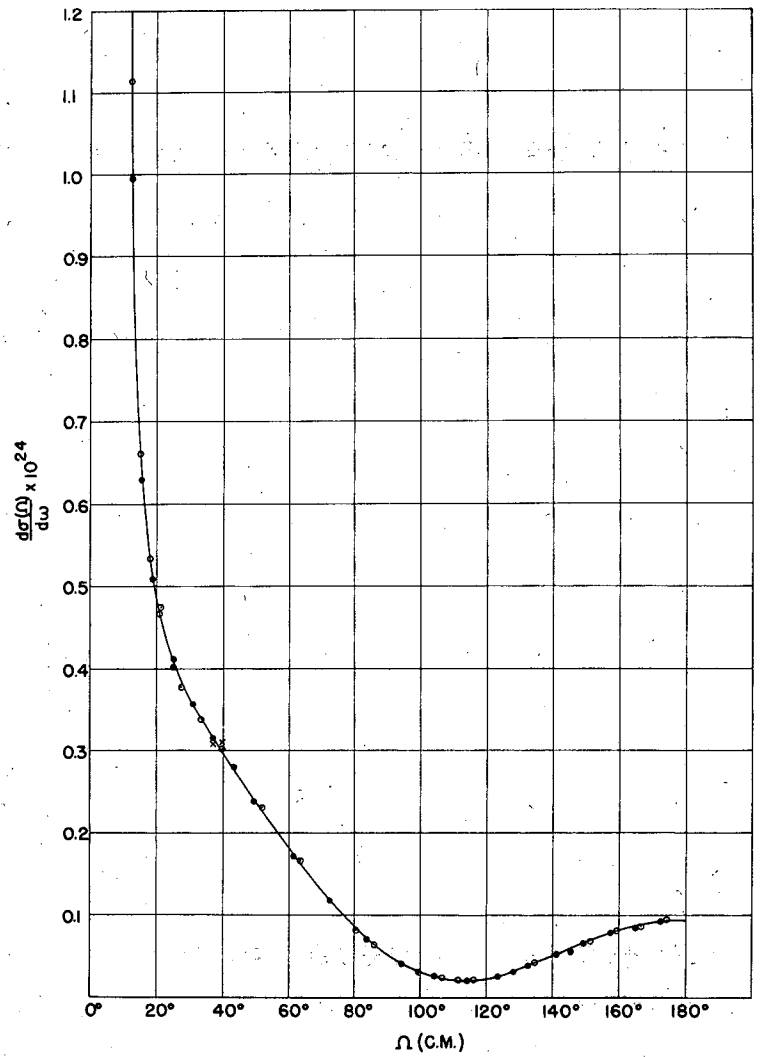

The DIFFERENTIAL CROSS SECTION for the SCATTERING of 9.5 Mev. PROTONS from HELIUM

Figure 21.

MU 2285

TABLE B

MEASURED CROSS SECTIONS AS A FUNCTION OF ANGLE IN THE CENTER-OF-MASS SYSTEM AT 9.48 MEV INCIDENT PARTICLE ENERGY

(Laboratory angles shifted 0.2 degrees)

θ	Ω	do (Ω)/dω (barns)				
		1	2	4	5	6
9.8°	12.2°		1.1415			
10.2	12.8		0.9947			
12.3	15.3		0.6596			
12.7	15.9		0.6294			
14.8	18.4		0.5336			
15.2	19.0		0.5086			
17.3	21.5		0.4754			0.4662
20.2	25.2		0.4126			0.4018
22.3	27.7					0.3780
25.2	31.3					0.3580
27.3	33.9					0.3382
30.2	37.4			0.3116		0.3076
32.3	40.0			0.3016		0.3099
35.2	43.5			0.2804		
40.2	49.5			0.2392		
42.3	52.0			0.2322		
50.2	61.3			0.1719		
52.3	63.7			0.1668		
60.2	72.7	0.1195				
67.3	80.6				0.0822	
70.2	83.8				0.0715	
72.3	86.1				0.0653	
80.2	94.5				0.0431	
85.2	99.6				0.0322	
90.2	104.7				0.0278	
92.3	106.8				0.0251	
97.3	111.7				0.02302	
100.2	114.4				0.0220	
102.3	116.4				0.02302	
110.2	123.8				0.0273	
115.2	128.3				0.0333	
120.2	132.7				0.0392	
122.3	134.5				0.0423	
130.2	141.2				0.0527	
135.2	145.4				0.0562	
140.2	149.4				0.0669	
142.3	151.1			0.0686		
150.2	157.3			0.0802		
152.3	159.0			0.0809		
160.2	165.0			0.0854		
162.3	166.7			0.0867		
170.2	172.6			0.0922		
172.3	174.2			0.0967		

accuracy and the internal consistency of the data above and below this point.

To facilitate comparison of the results of this experiment with that of earlier work at lower energies, the differential cross sections at 1.49-, 2.02-, 2.53-, and 3.58 Mev are compared with the curve at 9.48 Mev in Fig. 22. The lower energy data is that of Freier et al[20] taken at Minnesota. It is interesting to note the similarity in shape of the angular distribution curves at 3.58 Mev and 9.48 Mev. The minima occur at approximately the same angle in the center-of-mass system and the two curves are nearly parallel at angles greater than about 60 degrees. As expected, however, the Coulomb scattering becomes significant at a lower scattering angle for the higher energy case. It is also interesting to note the sudden change in shape of the angular distribution between 1.49 Mev and 2.02 Mev. Actually the change in shape occurs between 1.70 Mev and 2.02 Mev as indicated in reference (3). (This curve was left out of Fig. 22 to avoid confusion with the other data). This change in shape appears to occur near the resonance energy of the Li^5 state at 1.8 Mev[21]. For comparison purposes the calculated curve for ordinary proton-helium Coulomb scattering is plotted in the same figure.

The techniques used in obtaining the data from the nuclear plates were discussed in Capter IV. Certain corrections were made to the raw data to correct for the effect of the absorbers used at the forward angles, for inherent background and for scattering from impurities in the gas. The correction for absorbers at the forward angles was made for the loss of particles in a given swath width due to multiple scattering in the absorber. The amount of the correction was determined from data supplied by the Microscopy Laboratory at Los Alamos. This data was obtained using the graphical method

---

[20] See reference (3).

[21] W. F. Hornyak, T. Lauritsen, P. Morrison, and W. F. Fowler, Rev. Mod. Phys. 22, 291 (1950).

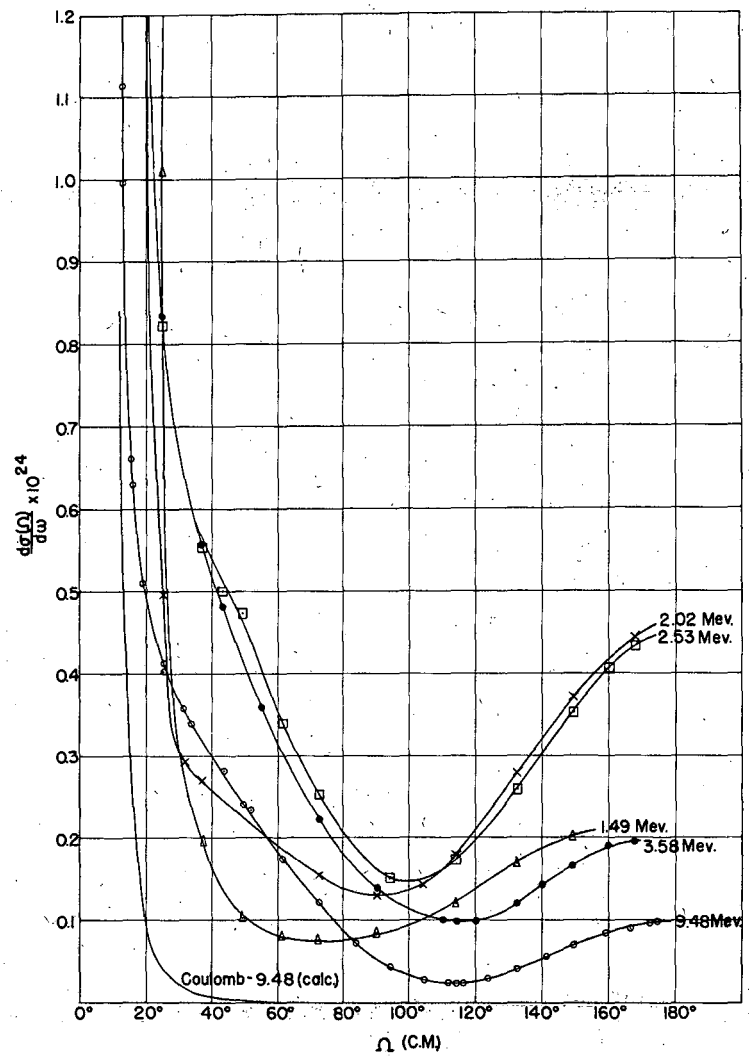

The DIFFERENTIAL CROSS SECTION
for the SCATTERING of PROTONS from
HELIUM for VARIOUS ENERGIES

Figure 22.

MU 2286

devised by Dickinson and Dodder[22]. The correction amounted to approximately 6 percent for the 0.008 inch aluminum absorbers used. In addition, corrections were necessary for the scattering of protons from water vapor (oxygen) given off from the plates and from impurities, mainly nitrogen, in the scattering gas. The former is called background scattering and the latter, impurity scattering.

The necessary background corrections were determined from the analysis of plates exposed in a background run. The number of tracks per centimeter swath width which would have been included in the normal counting at each angle was determined from the range analysis of the background plate at the same angle. This number was normalized for the rate of rise taken prior to each run as compared to that of the background run and, for the integrated current used. The correction amounted to less than 1 percent at 10 degrees and above 20 degrees was small enough (< 0.03 percent) to be neglected.

The correction for impurity scattering was based on pure Coulomb scattering. By calculating the expected mean proton ranges of particles scattered from nitrogen and comparing this with the accepted range for counting tracks on each plate, the angles over which a correction had to be applied were determined. It was found that below 37.5 degrees, particles scattered from nitrogen or oxygen would not be resolved from the main proton peak. As a matter of confirmation of this, tracks of range longer than the accepted were noted on plates at angles from 40 degrees and above. These tracks were not counted.

In order to determine the amounts of impurities in the helium gas used, an analysis was made of the gas by Dr. Amos Newton of the Radiation Laboratory using a Consolidated 180° Focusing Mass Spectrograph. The results of this

---

22 W. C. Dickinson and D. C. Dodder, Los Alamos Report LA 1182, (1950).

analysis showed the primary contaminants to be hydrogen - 0.02 percent, nitrogen - 0.02 percent, and oxygen - 0.01 percent. Using these figures and the cross sections for the Coulomb scattering of protons from nitrogen and oxygen (see Appendix IV) corrections were determined for impurity scattering. These amounted to approximately one-half percent at 10 degrees and were completely negligible at 20 degrees. No corrections were necessary for the hydrogen present due first to the smaller proton-proton scattering cross section in this energy range[23] and, secondly, to the fact that the ranges would be resolved above 15 degrees.

Above 20 degrees there were no other corrections made to the number of tracks counted per centimeter swath width. One other source of background is open to question, however. This enters in the low energy "tail" of the range distribution peak. The incident proton beam was not monoenergetic and had a low energy tail from the nature of its production. This would, likewise, introduce a low energy tail on the range distribution. On the other hand, protons scattered by the slits would lose some energy and would contribute to this effect. In making the selection of the lower energy limit for acceptible tracks on theplate, this had to be considered. From an examination of the range distribution curves for each plate, it appears that the selection of ranges used would take care of this effect. Further corrections, if any, would be less than 1 percent and open to considerable error. Thus, none were made. The effect of multiple scattering in the gas was also investigated. The loss of particles due to this effect was found to be completely negligible. The largest effect would have been at the backward angles where the scattered particle energy is of the order of 3 Mev. Calculations (based on Reference 22) indicated that less

---

[23] R. R. Wilson, Phys. Rev. 71, 384 (1947).

than one percent of the particles would be deviated by only a few thousandths of a degree and, hence, the effect was completely negligible.

As indicated previously, the relative accuracy of points obtained on the same run should be good to the standard deveiation of the counting statistics. This was approximately 2 percent for each point. The absolute accuracy of the data will depend, in addition, on the experimental accuracy in obtaining the data. The factors whose errors enter into the overall accuracy of the data are the current integration, the gas pressure and temperature measurement, personnel factors in reading the plates, the calibration of the eyepiece reticule in the microscope and the measurement of geometrical factors of the multiplate camera.

The accuracy of the current integration depended primarily on the calibration of the integrating condenser. The method used for this has already been discussed. The capacity of the standard capacitor used was given to ± 0.1 percent. From the spread of values obtained in making the calibration, the integrating capacity was given to ± 0.5 percent. A precision voltmeter was used to measure the voltage and the zero drift of the electrometer circuit was included. Thus, a probable error of 1 percent appears to be a conservative figure.

Measurements of the gas pressure were made with a precision cathetometer by at least two observers. From the reproducibility of the measurements, and the necessary application of a correction for expansion of the mercury in the manometer, the probable error to be assigned to the gas pressure measurement is ± 0.2 percent. The temperature of the gas was measured to ± 0.1 degree out of 25 to 30 degrees giving a probable error of ± 0.5 degrees.

The probable error in measurement of Y, the yield on each plate is somewhat difficult to assign. Frequent checks of the count on a single

swath by two observers indicated, however, an overall accuracy of better than 1 percent. Since these checks were made under possibly very favorable conditions, a more conservative figure for the probable error due to personnel factors would be ± 1.5 percent. For the calibration of the reticule, from the spread in values obtained, a probable error ± 0.4 percent can be assigned.

The measurements of geometrical factors for the nuclear plate camera have an estimated probable error of less than 1 percent. These are: a,b - 0.5 percent; ℓ- 0.1 percent; L as measured on the plate - 0.1 percent.

The resulting root mean square probable error for the measurements which enter into the cross section calculation is 2.06 percent. Considering the average statistical accuracy of 2 percent, a figure of ± 2.9 percent for the absolute standard error can be assigned to all points in the angular range of 25 - 175 degrees (CM). The point at 72.7 degrees (CM) due to its statistical accuracy of 4.3 percent can be assigned a probable error of ± 4.75 percent. At the more forward angles where large corrections are needed for the absorbers, an absolute standard error ± 5.0 percent can be assigned.

With regard to a possible excited state in Li^5 being observed, the range analyses of each plate were examined for possible lower energy proton peaks. None were found. In addition, during the counting of some of the plates, possible groups of particles of shorter range were looked for but here again there were no particular ranges that appeared to occur more often than others. Thus, at the incident particle energy used in this experiment and under the experimental conditions used, no excited state of ~~Li^5~~ He^4 was observable.

APPENDIX I

THE CRITCHFIELD FORMULA

The formula for the differential cross-section per unit solid angle in terms of the yield of particles in a swath of width w on the photographic detector was discussed in Capter II, section 1. The results of the computation of the quantity I, defined by

$$I = \iint \frac{w \sin\phi}{R^2} \, dy \, dx ,$$

where given there. The derivation of this result was originally worked out by Dr. C. L. Critchfield, Professor of Physics at the University of Minnesota and Consultant to the Los Alamos Scientific Laboratories. The following computation is based on his notes.

Let the path of the scattered particle be along the line R (see Fig. 23A). Assume the particle is scattered from a point at a distance y from the scattering center (defined by the intersection of the center line through the slits with the beam axis). The particle enters the emulsion at a point which is at a distance x from the center of the plate (determined by the intersection of the center line through the slits with the beam axis). Then a strip on the plate of width w will receive a number of scattered particles which will be proportional to

$$d^2I = w dx \, dy \, \sin\phi / R^2 ,$$

where ϕ is the angle between R and the detector plate P. The total number of particles detected in the swath w will then be proportional to the integral of this expression over x and y. The limits of the integration will be determined by the half widths of the defining slits, i.e., a and b.

It would be more convenient to transform to coordinates which have independent limits, thus we transform from x and y coordinates to coordinates

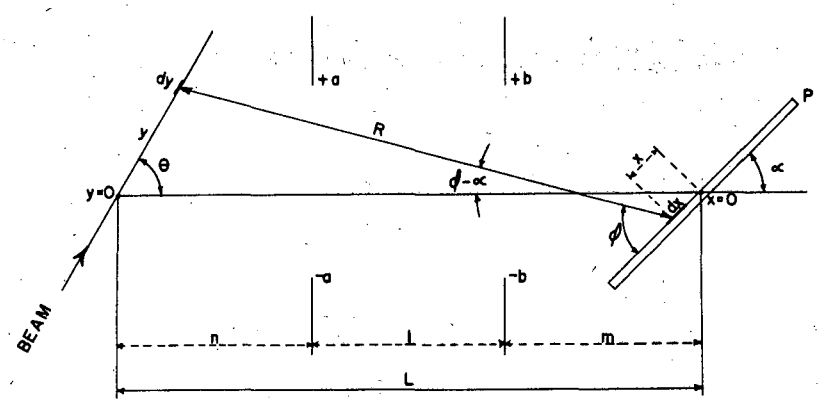

SLIT SYSTEM GEOMETRY

Figure 23 A

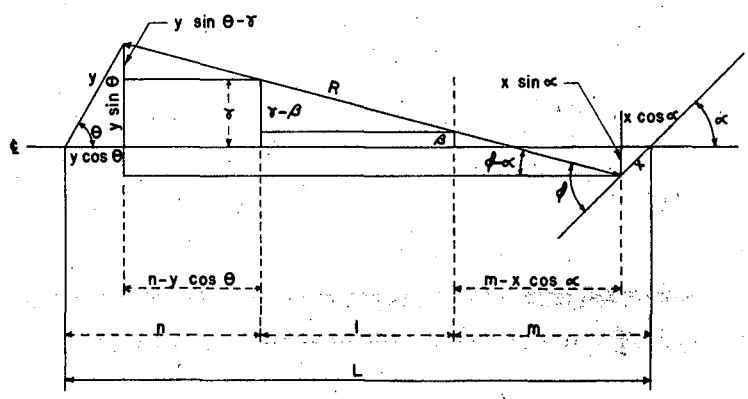

SLIT SYSTEM GEOMETRY

SHOWING EQUIVALENT SIMILAR TRIANGLES

Figure 23 B

MU 2283

in the planes of the slits. Let γ be the distance from the axis at which R passes through the first or inner slit. Let β be the same coordinate for the second slit. We obtain expressions for x and y in terms of γ and β and the geometrical constants from the similar triangles formed by the slit detector geometry. (See Fig. 23B) We must also express $\sin \phi$ in terms of the angles θ and α and the distance R in terms of γ, β, and functions of θ and α.

From the geometry we have the following relations:

$$\tan(\phi - \alpha) = \frac{y \sin\theta - \gamma}{n - y\cos\theta} = \frac{\gamma-\beta}{\ell} = \frac{\beta + x\sin\alpha}{m - x\cos\alpha} \tag{A}$$

$$\frac{R}{L - y\cos\theta - x\cos\alpha} = \frac{\sqrt{\ell^2 + (\gamma-\beta)^2}}{\ell} \tag{B}$$

$$\sin(\phi-\alpha) = \frac{\gamma-\beta}{\sqrt{\ell^2 + (\gamma-\beta)^2}}\ ; \qquad \cos(\phi-\alpha) = \frac{\ell}{\sqrt{\ell^2 + (\gamma-\beta)^2}}\ . \tag{C}$$

From these relations the necessary relations for x, y, R and $\sin\theta$, are obtained. These are:

$$X = \frac{m(\gamma-\beta) - \beta\ell}{\ell\sin\alpha + (\gamma-\beta)\cos\alpha} \tag{1}$$

$$y = \frac{n(\gamma-\beta) + \gamma\ell}{\ell\sin\theta + (\gamma-\beta)\cos\alpha} \tag{2}$$

$$R = \frac{1}{\ell}\left[L - y\cos\theta - x\cos\alpha\right]\sqrt{\ell^2 + (\gamma-\beta)^2} \tag{3}$$

$$\sin\phi = \sin\left[(\phi-\alpha) + \alpha\right] = \frac{(\gamma-\beta)\cos\alpha + \ell\sin\alpha}{\sqrt{\ell^2 + (\gamma-\beta)^2}}\ . \tag{4}$$

The next step is the evaluation of the Jacobian for the transformation of the differential elements, i.e.

$$J(xy) = \frac{\partial(xy)}{\partial(\gamma\beta)} = \frac{\partial x}{\partial\gamma}\frac{\partial y}{\partial\beta} - \frac{\partial x}{\partial\beta}\frac{\partial y}{\partial\gamma}\ .$$

From equations 1 and 2 we obtain by partial differentiation:

$$\frac{\partial x}{\partial \gamma} = \frac{m - x\cos\alpha}{\ell\sin\alpha + (\gamma-\beta)\cos\alpha} \quad ; \frac{\partial x}{\partial \beta} = \frac{-(m+\ell) + x\cos\alpha}{\ell\sin\alpha + (\gamma-\beta)\cos\alpha}$$

$$\frac{\partial y}{\partial \gamma} = \frac{n + \ell - y\cos\theta}{\ell\sin\theta + (\gamma-\beta)\cos\theta} \quad ; \frac{\partial y}{\partial \beta} = \frac{-n + y\cos\theta}{\ell\sin\theta + (\gamma-\beta)\cos\theta}$$

For the Jacobian we have

$$J(xy) = \frac{\partial(xy)}{\partial(\gamma\beta)} = \frac{\begin{vmatrix} m - x\cos\alpha & n + \ell - y\cos\theta \\ -(m+\ell) + x\cos\alpha & -n + y\cos\theta \end{vmatrix}}{\left[\ell\sin\theta + (\gamma-\beta)\cos\theta\right]\left[\ell\sin\alpha + (\gamma-\beta)\cos\alpha\right]} .$$

Expanding the numerator gives

$$J(xy) = \frac{\left[L - x\cos\alpha - y\cos\theta\right]\ell}{\left[\ell\sin\theta + (\gamma-\beta)\cos\theta\right]\cdot\left[\ell\sin\alpha + (\gamma-\beta)\cos\alpha\right]} . \qquad (5)$$

The expression for d^2I can now be evaluated;

$$d^2I = \frac{w\sin\phi}{R^2} \; J(xy)\, d\gamma\, d\beta . \qquad (6)$$

Substituting equations (3), (4), and (5) into (6) gives

$$d^2I = \frac{w\ell^3 \left[(\gamma-\beta)\cos\alpha + \ell\sin\alpha\right] d\gamma\, d\beta}{\left[\ell^2+(\gamma-\beta)^2\right]^{3/2}\left[L-y\cos\theta-x\cos\alpha\right]\left[\ell\sin\theta+(\gamma-\beta)\cos\theta\right]\left[\ell\sin\alpha-(\gamma-\beta)\cos\alpha\right]} .$$

NOTE: the similar bracketer terms in numerator and denominator are not cancelled out to make the treatment simpler.

Let

$$X = \left[L-y\cos\theta - x\cos\alpha\right]\left[\ell\sin\theta - (\gamma-\beta)\cos\theta\right]\left[\ell\sin\alpha-(\gamma-\beta)\cos\alpha\right] ,$$

which makes the denominator $X \cdot \left[\ell^2 + (\gamma-\beta)^2\right]^{3/2}$. Substituting in X for x and y and expanding yields the final expression for X:

$$X = L\,\ell\sin\theta\,\sin\alpha\left\{\ell + (\gamma-\beta)\cot\alpha + \frac{m(\gamma-\beta)-\beta\ell}{L}\left[\cot\theta - \cot\alpha\right]\right\} ,$$

and

$$d^2I = \frac{w\ell^3\left[(\gamma-\beta)\cos\alpha + \ell\sin\alpha\right]\,d\gamma\,d\beta}{X\left[\ell^2 + (\gamma-\beta)^2\right]^{3/2}}$$

$$= \frac{w\ell^3\left[\ell + (\gamma-\beta)\cot\alpha\right]\,d\gamma\,d\beta}{L\ell\sin\theta\left[\ell^2 + (\gamma-\beta)^2\right]^{3/2}\left\{\ell + (\gamma-\beta)\cot\alpha + \frac{m(\gamma-\beta)-\beta\ell}{L}\left[\cot\theta - \cot\alpha\right]\right\}} .$$

Further simplification is possible by setting

$$P = \frac{m(\cot\alpha - \cot\theta)}{L};\quad Q = \frac{(m+\ell)(\cot\alpha - \cot\theta)}{L} . \qquad (7)$$

Then

$$d^2I = \frac{w\ell^2}{L\ell^3\sin\theta\left[1 + \left(\frac{\gamma-\beta}{\ell}\right)^2\right]^{3/2}} \cdot \frac{\left[\ell + (\gamma-\beta)\cot\alpha\right]\,d\gamma\,d\beta}{\ell + (\gamma-\beta)\cot\alpha - (P\gamma - Q\beta)} ,$$

and so

$$d^2I = \frac{w\,d\gamma\,d\beta}{L\ell\sin\theta\left[1 + \left(\frac{\gamma-\beta}{\ell}\right)^2\right]^{3/2}} \cdot \frac{1}{1 - \frac{P\gamma - Q\beta}{\ell + (\gamma-\beta)\cot\alpha}} .$$

These two terms can be expanded in series form. The first term is of the form

$$K\,\frac{1}{(1+u)^{3/2}} = K\left(1 - 3/2\,u + 15/8\,u^2 + \cdots\right) ,$$

while the second term is of the form $\frac{1}{1-u} = 1 + u + u^2 + \cdots$.

Such an expansion gives

$$d^2I = \frac{w\,d\gamma\,d\beta}{L\ell\sin\theta}\left[1 - \frac{3}{2}\left(\frac{\gamma-\beta}{\ell}\right)^2 + \frac{15}{8}\left(\frac{\gamma-\beta}{\ell}\right)^4 + \cdots\right]\left[1 + \frac{P\gamma-Q\beta}{\ell+(\gamma-\beta)\cot\alpha} + \left(\frac{\beta\gamma-Q\beta}{\ell+(\gamma-\beta)\cot\alpha}\right)^2 + \cdots\right] .$$

The second bracket term can be expanded further:

first term: $\frac{P\gamma-Q\beta}{\ell+(\gamma-\beta)\cot\alpha} = \frac{P\gamma-Q\beta}{\ell}\cdot\frac{1}{1+\frac{\gamma-\beta}{\ell}\cot\alpha} = \frac{P\gamma-Q\beta}{\ell}\left\{1 + \frac{\gamma-\beta}{\ell}\cot\alpha + \left(\frac{\gamma-\beta}{\ell}\right)^2\cot^2\alpha + \cdots\right\}$,

second term: $= \left(\frac{P\gamma-Q\beta}{\ell}\right)^2\left\{1 - 2\,\frac{\gamma-\beta}{\ell}\cot\alpha + 3\left(\frac{\gamma-\beta}{\ell}\right)^2\cot^2\alpha + \cdots\right\}$.

Retaining only second order terms in γ and β gives:

$$d^2I = \frac{w\, d\gamma d\beta}{L\ell \sin\theta}\left[1 - \frac{3}{2}\frac{(\gamma-\beta)^2}{\ell^2}\right]\left[1 + \frac{P\gamma-Q\beta}{\ell}\left\{1 - \frac{\gamma-\beta}{\ell}\cot\alpha\right\} + \left(\frac{P\gamma-Q\beta}{\ell}\right)^2\right]$$

$$= \frac{w\, d\gamma\, d\beta}{L\ell\sin\theta}\left[1 - \frac{3}{2}\left(\frac{\gamma-\beta}{\ell}\right)^2 + \frac{P\gamma-Q\beta}{\ell} - \left(\frac{P\gamma-Q\beta}{\ell}\right)\left(\frac{\gamma-\beta}{\ell}\cot\alpha\right) + \left(\frac{P\gamma-Q\beta}{\ell}\right)^2\right] .$$

Expanding the integrating over γ from $-a$ to $+a$ and over β from $-b$ to $+b$ gives the final result for I:

$$I = \frac{4a\, bw}{L\ell\sin\theta}\left\{1 - \frac{a^2+b^2}{2\ell^2} - \frac{Pa^2+Qb^2}{3\ell^2}\cot\alpha + \frac{Pa^2+Qb^2}{3\ell^2}\right. ,$$

with

$$P = \frac{m(\cot\alpha - \cot\theta)}{L} , \quad Q = \frac{(m+\ell)(\cot\alpha - \cot\theta)}{L} .$$

This treatment, it should be noted, does not include corrections for the finite width of the beam, for variations in $d\sigma(\theta)/d\omega$ with R or for the finite swath width w. The first correction has been idscussed in Capter 2 and can be neglected. Likewise, the third correction is also negligible. Concerning the second, Critchfield says, "Of the neglected corrections, the only one that might amount to something is the correction to the differential cross section for different angles of scattering (through the slit system)." Thus using $\sigma(\theta)$ for $d\sigma(\theta)/d\omega$ an expansion can be made in Taylor's series form

$$\sigma(\theta + \phi-\alpha) = \sigma(\theta) + (\phi-\alpha)\,\sigma'(\theta) + \text{--}$$
$$\simeq \sigma(\theta) + (\gamma-\beta)/\ell\ \sigma'(\theta)$$
$$= \sigma(\theta)\ \left\{1 + (\gamma-\beta)/\ell\ \ \sigma'\theta/\sigma\theta\right\},$$

since $\phi-\alpha$ is small and

$$\tan(\phi-\alpha) = (\phi-\alpha) = \gamma-\beta/\ell .$$

In its interaction with the term $(P\gamma-\phi\beta)/\ell$ in the expression for d^2I above,

this correction leads to the additional correction term

$$1 + \frac{Pa^2 + \emptyset b^2}{3\ell^2} \quad \frac{\sigma'(\theta)}{\sigma\ (\theta)} ,$$

since indeed $\sigma'(\theta)/\sigma(\theta)$ will be a relatively small term, it will make this second order correction term even smaller and hence completely negligible. Calculations also show that the maximum value of the correction to the simplified cross section formula used in this experiment is less than 0.1 percent. This occurs in the neighborhood of 90° in the laboratory system.

APPENDIX II

COLLISION MECHANICS FOR PROTON-HELIUM SCATTERING

The general expressions for certain of the fundamental quantities in elastic scattering and their transformation to center-of mass (C.M.) coordinates have been discussed in Chapter II. These ralations will be derived below based on classical non-relativistic mechanics.

Consider a particle of mass M_1 initial velocity V_o and initial energy E_o incident on a stationary particle (in the laboratory system) of mass M_2. Assuming elastic scattering to occur, the products will be the two particles of mass M_1 and M_2 but these move off with new velocities V_1 and V_2 and energies E_1 and E_2 respectively in the laboratory system. Following somewhat the notation of Carlson et al[24]. The scattering process can be pictured as shown below:

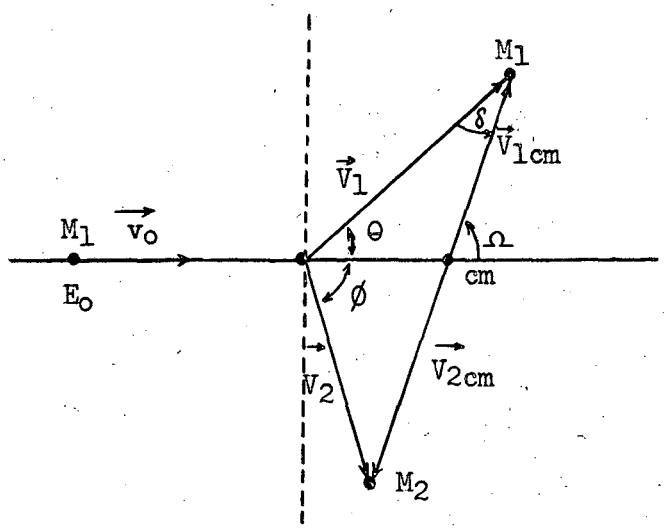

It is convenient in dealing with scattering data to refer the cross sections to the system of coordinates in which the center of mass of the two particles is at rest. In the figure then θ is the proton scattering angle in the laboratory system while Ω is the proton angle in the center-of-mass system. In this system, it should be noted that the two particles are

[24] B. Carlson, M. Goldstein, L. Rosen, and D. Sweeney, La-723, (1949).

approaching each other and after the collision they go off in exactly opposite directions.

Applying the conservation of momentum to the process we note that the momentum before the collison is the same in either system so:

$$M_1 \vec{V}_o = (M_1 + M_2) \vec{V}_{cm} ,$$

which gives

$$\vec{V}_{cm} = \frac{M_1}{M_1 + M_2} \vec{V}_o = \frac{M_1}{M_1 + M_2} \sqrt{\frac{2 E_o}{M_1}} . \qquad (1)$$

Since $M_1 = 1$ and $M_2 = 4$ in the proton helium case, then

$$\vec{V}_{cm} = 1/5 \vec{V}_o = 1/5 \sqrt{2 E_o} . \qquad (2)$$

From the vectors in the figure we note that the following relations hold before the collision:

(1) Velocity of the proton in the C.M. system is

$$\vec{V}_{1cm} = \vec{V}_o - \vec{V}_{cm} \qquad (3)$$

(2) The velocity of the target nucleus in the C. M. system before collision is $\vec{V}_{2cm} = - \vec{V}_{cm}$.

These give

$$\vec{V}_{Hecm} = - 1/5 \vec{V}_o, \text{ and } \vec{V}_{pcm} = - 4 \vec{V}_{Hecm} = 4/5 \vec{V}_o . \qquad (4)$$

Applying the conservation of energy during the collision gives the condition that the kinetic energy in the center-of-mass system is conserved during the collision. The total kinetic energy after the collision is equal to the available kinetic energy before the collision.

Thus, $1/2 M_1 V_{1cm}^2 + 1/2 M_2 V_{2cm}^2 =$ incident energy less the kinetic energy of the center-of-mass. This latter quantity is obtained from:

$$KE_{cm} = 1/2 (M_1 + M_2) V_{cm}^2 .$$

Substituting from Equation (1) gives

$$KE_{cm} = \frac{M_1}{M_1 + M_2} E_o . \qquad (5)$$

For the proton-helium case, $KE_{cm} = 1/5\ E_o$.

The expression for the conservation of energy becomes

$$1/2\ M_1\ V_{1cm}^{\ 2} + 1/2\ M_2\ V_{2cm}^{\ 2} = E_o - \frac{M_1}{M_1 + M_2} E_o = \frac{M_2}{M_1 + M_2} E_o\ . \qquad (6)$$

To determine the center-of-mass angle from the known laboratory angle for the scattering process, the geometry is again referred to. Applying the law of sines to the upper triangle

$$\frac{\sin \theta}{V_{1cm}} = \frac{\sin \delta}{V_{cm}}\ , \qquad (7)$$

and likewise $\theta + \delta = \Omega$ the center-of-mass angle. From equations (1) and (3) the velocity of the incident particle in the center-of-mass system becomes

$$V_{1cm} = \sqrt{\frac{2\ E_o}{M_1}} - \frac{M_1}{M_1 + M_2} \sqrt{\frac{2\ E_o}{M_1}} = \frac{M_2}{M_1 + M_2} \sqrt{\frac{2\ E_o}{M_1}}\ . \qquad (8)$$

Substituting for V_{1cm} and V_{cm} in Equation (7) gives

$$\sin\ \delta = \frac{M_1}{M_2}\ \sin \theta.$$

Thus, $\Omega = \theta + \sin^{-1} (1/4 \sin \theta)$ (9)

for the proton helium collision.

In determining the relative intensity of the scattered particles in the two coordinate systems, note that these are inversely proportional to the elements of solid angle in the two systems. Thus

$$I\ (\Omega)\ 2\ \pi\ \sin \Omega\ d\ \Omega = I\ (\theta)\ 2\ \pi\ \sin \theta\ d\ \theta$$

and

$$\frac{I\ (\Omega)}{I\ (\theta)} = \frac{\sin \theta}{\sin \Omega}\ \frac{d\ \theta}{d\ \Omega}\ . \qquad (10)$$

In order to convert the cross section in the laboratory system to

the center-of-mass system, the right side of this expression must be evaluated. From the figure again,

$$V_{cm} = V_1 \cos \theta - V_{1cm} \cos \Omega \,, \tag{11}$$

$$\frac{V_{1cm}}{\sin \theta} = \frac{V_1}{\sin \Omega} \,, \tag{12}$$

and from the law of cosines

$$V_1^2 = V_{cm}^2 + V_{1cm}^2 + 2\, V_{cm}\, V_{1cm} \cos \Omega \,. \tag{13}$$

Substituting for V_{1cm}, V_1 and V_{cm} in Equation (11) gives

$$\cos \Omega = \frac{M_1 + M_2}{M_2} \sqrt{\frac{E_1}{E_o}} \cos \theta - \frac{M_1}{M_2} \,. \tag{14}$$

Differentiating this with respect to Ω considering E_1/E_2 as a function of Ω gives

$$-\sin \Omega = - \frac{M_1 + M_2}{M_2} \sin \theta \frac{d\theta}{d\Omega} \sqrt{\frac{E_1}{E_o}} + 1/2 \frac{M_1 + M_2}{M_2} \cos \theta \left(\frac{E_1}{E_o}\right)^{-1/2} \frac{d}{d\Omega}\left(\frac{E_1}{E_o}\right) .$$

To determine E_1/E_o as a function of Ω, V_{cm} and V_{1cm} are substituted into expression (13). This gives

$$\frac{E_1}{E_o} = A + B + 2\sqrt{A\,B} \cos \Omega \,, \tag{15}$$

where $A = \dfrac{M_1^2}{(M_1 + M_2)^2}$ and $B = \dfrac{M_2^2}{(M_1 + M_2)^2}$.

Then

$$\frac{d}{d\Omega}\left(\frac{E_1}{E_o}\right) = 2\sqrt{AB} \sin \Omega \,.$$

This gives

$$- \sin \Omega = -\sqrt{\frac{E_1/E_o}{B}} \sin \theta \frac{d\theta}{d\Omega} - 1/2 \sqrt{\frac{E_1/E_o}{B}} \cos \theta \; 2\sqrt{AB} \sin \Omega \,.$$

Then the final expression for the intensity ratio is

$$\frac{I(\Omega)}{I(\theta)} = \frac{\sin\theta\, d\theta}{\sin\Omega\, d\Omega} = \frac{\sqrt{B}\,(E_1/E_o)^{1/2} - \sqrt{A\,B}\cos\theta}{E_1/E_o} \quad . \tag{16}$$

To determine the energy ratio E_1/E_o in terms of the laboratory scattering angle θ equation (12) gives

$$\sin\theta = \frac{V_{1cm}}{V_1}\sin\Omega \quad .$$

and to determine an alternate expression for $\cos\Omega$ the expressions for V_1 and V_{1cm} are substituted giving

$$\sin\theta = \sqrt{B}\,\sqrt{E_o/E_1}\,\sin\Omega\ ,$$

and from this

$$\cos\Omega = \sqrt{1 - (1/B)\ (E_1/E_o)\ \sin^2\theta} \quad . \tag{17}$$

Substituting this expression for $\cos\Omega$ into Equation (15) gives

$$E_1/E_o = A + B + 2\ \sqrt{AB - A\ E_1/E_o\ \sin^2\theta} \quad . \tag{18}$$

The solution of this for E_1/E_o gives

$$E_1/E_o = A\ (\cos\theta \pm \sqrt{B/A - \sin^2\theta})^2 . \tag{19}$$

In the proton-helium scattering case the incident nucleus is lighter than the target nucleus and it is scattered with a single discrete energy in an elastic encounter. Thus, only one solution for E_1/E_o has physical significance. This must be the solution with the positive sign as can be shown by the result when θ goes to zero at which point $E_1 = E_o$. Substituting the numerical values for A and B gives

$$E_p/E_o = 1/25\ \left(\cos\theta + \sqrt{16-\sin^2\theta}\right)^2, \tag{20}$$

and

$$\frac{I(\Omega)}{I(\theta)} = \frac{\sqrt{AB}\ \sqrt{B/A - \sin^2\theta}}{E_1/E_o} = \frac{4/25\ \sqrt{16-\sin^2\theta}}{E_p/E_o} \quad . \tag{21}$$

In a similar way the expression for E_2/E_o may be obtained. Applying the law of cosines to the lower triangle in the figure gives

$$V_2^2 = V_{cm}^2 + V_{2cm}^2 + 2\, V_{2cm}\, V_{cm} \cos \Omega . \tag{22}$$

Substituting for V_{2cm}, V_{cm} gives

$$V_2^2 = 2 \left(\frac{M_1}{M_1+M_2}\right)^2 \frac{2\, E_o}{M_1} - 2 \left(\frac{M_1}{M_1+M_2}\right)^2 \frac{2\, E_o}{M} \cos \Omega ,$$

and

$$\frac{1/2\, M_2 V_2^2}{E_o} = \frac{E_2}{E_o} = \frac{2\, M_1 M_2}{(M_1+M_2)^2} (1 - \cos \Omega) .$$

By a similar process to that used above, an expression is obtained for $\cos \Omega$ in terms of $\sin \phi$. The subsequent solution for E_2/E_o is

$$E_2/E_o = 4 \frac{M_1\, M_2}{M_1+M_2} \cos^2 \phi$$

and

$$E_{He}/E_o = 16/25 \cos^2 \phi .$$

APPENDIX III

EXPERIMENTAL DATA

TABLE A.

EXPERIMENTAL DATA FOR VARIOUS RUNS

RUN	GAS PRESSURE (cm Hg)	GAS TEMPERATURE (°C)	INTEGRATED CURRENT (micro-coulombs)
1	20.031	25.15	9.402
2	5.162	25.80	4.412
4	20.400	28.20	10.183
5	37.280	26.80	27.374
6	10.370	26.20	5.552

TABLE B.

GEOMETRICAL CONSTANTS OF THE MULTIPLATE CAMERA

Slit width: $a = b = 0.045'' = 0.1143$ cm.

Slit spacing: $\ell = 2.875'' = 7.55$ cm.

Plate angle: $= 11^\circ\ 46'$

Center axis: $L = 16.066$ cm + distance from edge of photographic plate to center-of-gravity of proton track density distribution.

TABLE C.

BEAM ENERGY VALUES

Run	Lab Angle	Range (Microns)	Energy (Mev)	E_o (Mev)	Run	Lab Angle	Range (Microns)	Energy (Mev)	E_o (Mev)
2	9.8	497	9.43	9.50	5	67.3	295	6.92	9.45
	10.2	492	9.37	9.45		70.2	292	6.88	9.63
	12.3	493	9.40	9.51		72.3	276	6.66	9.48
	12.7	498	9.45	9.57		80.2	243	6.18	9.44
	14.8	486	9.32	9.48		85.2	226	5.91	9.44
	15.2	478	9.24	9.40		90.2	210	5.65	9.44
	17.3	482	9.26	9.47		92.3	207	5.60	9.52
	20.2	473	9.18	9.47		97.3	190	5.32	9.46
						100.2	182	5.18	9.46
6	17.3	480	9.25	9.46		102.3	176	5.08	9.45
	20.2	479	9.24	9.53		110.2	157	4.74	9.44
	22.3	483	9.28	9.63		115.2	148	4.75	9.49
	25.2	468	9.12	9.57		120.2	137	4.36	9.42
	27.3	460	9.03	9.55		122.3	134	4.30	9.43
	30.2	444	8.85	9.48		130.2	120	4.03	9.36
	32.3	442	8.82	9.53		135.2	116	3.92	9.41
						140.2	107	3.76	9.30
4	30.2	440	8.80	9.42					
	32.3	440	8.80	9.51	4	142.3	108	3.77	9.42
	35.2	436	8.75	9.60		150.2	101	3.62	9.41
	40.2	416	8.52	9.60		152.3	100	3.60	9.44
	42.3	402	8.35	9.52		160.2	96	3.52	9.49
	50.2	368	7.92	9.50		162.3	94	3.47	9.41
	52.3	360	7.82	9.51		170.2	93	3.45	9.51
						172.3	92	3.41	9.43
1	60.2	331	7.44	9.60					

AVERAGE VALUES

Run	Number of Plates	Average (Mev)
1	1	9.60
2	8	9.48
4	14	9.48
5	17	9.45
6	7	9.53

Total for 47 plates: 9.48-Mev ± 0.15-Mev

APPENDIX IV

COULOMB SCATTERING

A. Proton-Helium Coulomb Scattering.

In order that a comparison can be made of the effect of the combined nuclear and Coulomb forces on the angular distribution of the scattered protons with that of Coulomb forces alone the cross section for Coulomb scattering is calculated here. The differential cross section in the center-of-mass system is given by the relation

$$\frac{d\sigma(\Omega)}{d\omega} = \left(\frac{Z_1 Z_2 e^2}{2\bar{M} V^2}\right)^2 \operatorname{cosec}^4\left(\frac{\Omega}{2}\right),$$

where $\bar{M}$ = reduced mass = $\frac{M_1 M_2}{M_1 + M_2}$, is the center-of-mass angle and V is the relative velocity. This may be rearranged into the form

$$\frac{d\sigma(\Omega)}{d\omega} = \left(\frac{Z_1 Z_2 e^2}{4 E_o}\right)^2 \frac{(M_1 + M_2)^2}{M_2^2} \operatorname{cosec}^4\left(\frac{\Omega}{2}\right).$$

For the proton-helium case $Z_1 = 1$, $Z_2 = 2$, $M_1 = 1$, and $M_2 = 4$.

This gives

$$\frac{d\sigma(\Omega)}{d\omega} = \frac{1}{16} \times \left(\frac{5}{4}\right)^2 \times \frac{4e^4}{E_o} \operatorname{cosec}^4\left(\frac{\Omega}{2}\right),$$

Introducing the value of 9.48-Mev for E_o, the differential cross section for the Coulomb scattering of 9.48-Mev protons from helium is

$$\frac{d\sigma(\Omega)}{d\omega} = 9.12 \times 10^{-5} \operatorname{cosec}^4\left(\frac{\Omega}{2}\right), \text{ barns.}$$

The cross sections for several angles that were used to plot the curve shown in Fig. 22 are given in Table I.

B. Proton-Nitrogen Coulomb Scattering.

In Chapter VII the corrections for impurity scattering were discussed. The differential cross sections for the scattering of 9.48-Mev protons from nitrogen nuclei are given here. One is concerned with corrections to the number of particles recorded on the photographic plates in the laboratory system. For this the differential cross section for Coulomb scattering in the laboratory system is

$$\frac{d\sigma(\theta)}{d\omega} = \left(\frac{Z_1 Z_2 e^2}{M_1 v^2}\right)^2 \operatorname{cosec}^3\theta \frac{\left[\cot\theta \pm \sqrt{\csc^2\theta - \left(\frac{M_1}{M_2}\right)^2}\right]^2}{\sqrt{\csc^2\theta - \left(\frac{M_1}{M^2}\right)^2}},$$

where v is the velocity of the incident proton and M_1 its mass.

Since the initial energy $E_o = 1/2\, M_1 v^2$ this may be written

$$\frac{d\sigma(\theta)}{d\omega} = \left(\frac{Z_1 Z_2 e^2}{2E_o}\right)^2 \operatorname{cosec}^4\theta \frac{\left[\cos\theta \pm \sqrt{1 - \left(\frac{M_1}{M_2}\right)^2 \sin^2\theta}\right]^2}{\sqrt{1 - \left(\frac{M_1}{M_2}\right)^2 \sin^2\theta}}.$$

For nitrogen $Z_2 = 7$ and $M_2 = 14$. Hence,

$$\frac{d\,\sigma(\theta)}{d\,\omega} = 0.00283 \operatorname{cosec}^4\theta \; \frac{\left[\cos\theta + \sqrt{1 - 1/196 \sin^2\theta}\right]^2}{\sqrt{1 - 1/196 \sin^2\theta}} .$$

The positive sign is used in the case of the proton-nitrogen case since the incident nucleus is lighter than the target nucleus. The cross sections used in calculating the correction for impurity scattering are given in Table II.

TABLE I

DIFFERENTIAL CROSS SECTION - COULOMB SCATTERING

Protons on Helium

C.M. Angle (degrees)	$\frac{d\sigma(\Omega)}{d\omega}$ (barns)
10	1.5800
11	1.0800
12	0.7640
15	0.3540
20	0.1000
25	0.0420
30	0.0200
35	0.0110
40	0.0067
45	0.0042

TABLE II

DIFFERENTIAL CROSS SECTION - COULOMB SCATTERING

Protons on Nitrogen

LAB Angle	$\frac{d\sigma(\theta)}{d\omega}$ (barns)
10.0	12.276
12.5	5.039
15.0	2.439
17.5	1.321
20.0	0.778
22.5	0.489
25.0	0.322
27.5	0.222
30.0	0.158
32.5	0.116
35.0	0.086

ACKNOWLEDGEMENTS

It is a great pleasure to acknowledge the encouragement, guidance and invaluable help that so many people have given to make this work possible. Sincere thanks are due to: Professor E. M. McMillan, Professor A. C. Helmholz and Professor J. G. Hamilton for their continued interest and guidance during the course of the entire program; Dr. Louis Rosen, for making this experiment possible by the use of the multiplate camera and for his help and guidance during the course of the work; Drs. J. C. Allred and R. O. Bondelid for their assistance in making the runs; Dr. Alice H. Armstrong for many helpful discussions and for the detailed answers given to the many questions that arose during the course of the work.

The reading of the photographic plates for a preliminary check was done in part at the Microscopy Laboratory at Los Alamos, chiefly by Mrs. J. Gammel and Mrs. M. Downs. Mrs. R. Gibbs and Mrs. M. Putnam assisted in the final counting of the tracks.

Thanks are also due to the many members of the 60" Cyclotron staff in Crocker Laboratory who have contributed in many ways towards the completion of this work.

This work was performed in part under the auspices of the Atomic Energy Commission.

BIBLIOGRAPHY

Allred, J. C., "The Differential Cross Section of the Reaction He^3 (dp)He^4 at 10.2 Mev Bombarding Energy and Search for Excited State in He^4", (1) Phys. Rev. 77, 753 (1950)A; (2) Los Alamos Laboratory Report LA-981 (1950) (UNCLASSIFIED).

Allred, J. C., L. Rosen, F. K. Tallmadge, and J. H. Williams, "Nuclear Multiplate Camera", Rev. Sci. Inst. 22, 191 (1951).

Chadwick, J., and E. S. Bieler, "The Collisions of Alpha Particles with Hydrogen Nuclei", Phil. Mag. 42, 923 (1921).

Critchfield, C. L., and D. C. Dodder, "Phase Shifts in Proton-Alpha Scattering", Phys. Rev. 76, 602 (1949).

Dickinson, W. C., and D. C. Dodder, "A Method for Evaluation of Multiple Scattering Effects in Charged Particle Experiments" Los Alamos Laboratory Report LA-1182, 1950 (UNCLASSIFIED).

Freier, George, Eugene Lampi, W. Sleator, and J. H. Williams, "Angular Distribution of 1- to 3.5-Mev Protons Scattered by He^4", Phys. Rev. 75, 1345 (1949).

Heydenburg, N. P., and R. B. Roberts, "Deuteron-Deuteron, Proton-Helium, and Deutron-Helium Scattering", Phys. Rev. 56, 1092 (1939).

Heydenburg, N. P., and N. F. Ramsey, "The Scattering of One- to Three Mev Protons by Helium", Phys. Rev. 60, 42 (1941).

Hornyak, W. F., T. Lauritsen, P. Morrison, and W. F. Fowler, "Energy Levels of Light Nuclei. III" Rev. Mod. Phys. 22, 291 (1950).

Kinoshita, S., "The Photographic Action of the Alpha-Particles Emitted from Radioactive Substances", Proc. Roy. Soc. 83A, 432, (1910).

Lattes, C. M. G., P. H. Fowler, and P. Cuer, "Range-Energy Relation for Protons and Alpha-Particles in the new Ilford 'Nuclear Research' Emulsions", Nature 159, 301 (1947).

Lattes, C. M. G., P. H. Fowler, and P. Cuer, "A Study of the Nuclear Transformations of Light Elements by the Photographic Method", Proc. Phys. Soc. (London) 59, 883 (1947).

Mohr, C. B. O., and G. E. Pringle, "The Scattering of Alpha-Particles in Helium, Hydrogen, and Deuterium", Proc. Roy. Soc. 160, 190 (1937).

Powell, C. F., and G. P. S. Occhialini, Nuclear Physics in Photographs, Oxford: The Clarendon Press, (1947).

Rosen, Louis, F. K. Tallmadge, and J. H. Williams, "Range Distribution of the Charged Particles from the D-D Reactions for 10 Mev Deuterons: Differential Elastic Cross Sections at 40 Degrees, 60 Degrees and 80 Degrees in the Center-of-Mass System", Phys. Rev. 76, 1283 (1949).

Rosen, L., and J. C. Allred, "Scattering of 10.4-Mev Deuterons by Hydrogen", Phys. Rev. 82, 777 (1951).

Shapiro, M. M., "Tracks of Nuclear Particles in Photographic Emulsions", Rev. Mod. Phys. 13, 58 (1941).

Webb, J. H., "Photographic Plates for Use in Nuclear Physics", Phys. Rev. 74, 511 (1948).

Wilkins, T. R., "The Response of Photographic Materials to Atomic Particles". J. App. Phys. 11, 35 (1940).

Williams, E. J., "Multiple Scattering of Fast Electrons and Alpha-Particles, and 'Curvature' of Cloud Tracks Due to Scattering" Phys. Rev. 58 292 (1940).

Wilson, R. R., "Proton-Proton Scattering at 10-Mev." Phys. Rev. 71, 384 (1947).

Yagoda, H., Radioactive Measurements with Nuclear Emulsions, John Wiley and Sons, (1949).